Precambrian Research 406 (2024) 107380

Contents lists available at ScienceDirect

Precambrian Research

journal homepage: www.elsevier.com/locate/precamres

Congo-São Francisco craton in Paleoproterozoic-Mesoproterozoic supercontinent Nuna

Johanna Salminen [a,b,*], David A.D. Evans [c], Ricardo I.F. Trindade [d], Richard Hanson [e], Ulf Söderlund [f], Richard E. Ernst [g], Martin B. Klausen [h], Ian Fieldhouse [i]

[a] Department of Geography and geosciences, University of Helsinki, P.O. Box 64, 00014 Finland
[b] Geological Survey of Finland, P.O. Box 96, FI-02151 Espoo, Finland
[c] Department of Earth & Planetary Sciences, Yale University, New Haven, CT 06520, USA
[d] Instituto de Astronomia, Geofísica e Ciências Atmosféricas, Universidade de São Paulo, São Paulo, SP, 055080-090, Brazil
[e] Department of Geological Sciences, Texas Christian University, Fort Worth, TX 76129, USA
[f] Department of Geology, Lund University, Lund223 62, Sweden
[g] Department of Earth Sciences, Carleton University, Ottawa K1S 5B6, Canada
[h] Department of Earth Sciences, Stellenbosch University, Private Bag X1, 7602 Matieland, RSA
[i] KoBold Metals, Sudbury, Canada

ARTICLE INFO

Keywords:
Paleomagnetism
Geochronology
Geochemistry
Congo-São Francisco craton
Nuna supercontinent

ABSTRACT

The location of the Congo-São Francisco (CSF) craton, one of the largest cratons in Proterozoic paleogeography, has been poorly constrained for the supercontinent Nuna interval (ca. 1800–1300 Ma). Initial models of Nuna suggested that the CSF craton was part of the Atlantica continent, together with Amazonia, West Africa, and perhaps Río de la Plata, as a separate continental block from other Nuna constituents. In other Nuna models the CSF craton has been placed adjacent to Baltica and Siberia, the core of Nuna, based mainly on ages of mafic magmatism and sparse paleomagnetic data. Through a geochemical, geochronological and paleomagnetic study of the WNW-trending Virei mafic dykes, which extend outward from the Mesoproterozoic Kunene Igneous Complex in southwest Angola, we provide a U-Pb baddeleyite age of 1385 ± 5 Ma, geochemical signatures, and a robust Mesoproterozoic paleomagnetic pole to test the CSF craton's placement within Nuna. Including our new pole with quality-filtered poles from the other cratons during the Nuna interval, we propose a refined Nuna model with (1) southwest Congo / west Siberia cratonic connection at 1700–1500 Ma, (2) proximity of Amazonia and West Africa cratons, and (3) connection of southwest Congo craton with northwest West Africa at 1380 Ma. Our proposed 1500–1380 Ma reconstructions are further supported by matching large igneous province (LIP) records from these crustal blocks. The new 1385 Ma Virei pole, when considered relative to an earlier CSF pole at ca. 1500 Ma, requires substantial azimuthal rotation (~85°) of CSF in the intervening time interval. To accommodate both the matching LIP records and paleomagnetic data from CSF and neighboring cratons in Nuna, we propose an interval of transform motion near the supercontinent's periphery prior to more widespread mid-Mesoproterozoic supercontinental breakup.

1. Introduction

The assembly and break-up of the Paleoproterozoic–Mesoproterozoic supercontinent Nuna (also known as Columbia) is considered by some to represent Earth's first supercontinent cycle, profoundly influencing Earth's geosphere, biosphere, ocean circulation, and atmosphere (e.g., Rogers, 1996; Rogers and Santosh, 2009; Nance et al., 2014; Condie et al., 2015). Paleogeographic reconstructions of the Nuna interval have shown significant advances in the last two decades (e.g., Pesonen et al., 2003; Evans, 2013; Pisarevsky et al., 2014; Pehrsson et al., 2016; Elming et al., 2021), based on global paleomagnetic data and geological correlations. There is common consensus that

* Corresponding author at: Department of Geography and geosciences, University of Helsinki, P.O. Box 64, 00014 Finland.
E-mail addresses: johanna.m.salminen@helsinki.fi (J. Salminen), david.evans@yale.edu (D.A.D. Evans), ricardo.trindade@iag.usp.br (R.I.F. Trindade), R.Hanson@tcu.edu (R. Hanson), ulf.soderlund@geol.lu.se (U. Söderlund), RichardErnst@cunet.carleton.ca (R.E. Ernst), klausen@sun.ac.za (M.B. Klausen), ian.fieldhouse@koboldmetals.com (I. Fieldhouse).

https://doi.org/10.1016/j.precamres.2024.107380
Received 16 December 2023; Received in revised form 26 March 2024; Accepted 28 March 2024
Available online 8 April 2024

Baltica, Laurentia and Siberia formed the core of the Nuna supercontinent (e.g., Gower et al., 1990; Salminen and Pesonen, 2007; Evans and Pisarevsky, 2008; Evans and Mitchell, 2011; Pisarevsky et al., 2014; Ernst et al., 2016; Mitchell et al., 2021), with proto-Australian cratons close to western margin of present-day Laurentia (e.g., Kirscher et al., 2020). Reconstructions of the Nuna supercontinent cycle (ca. 1800–1300 Ma) have been hampered by a lack of paleomagnetic data at key intervals. Notably, paleomagnetic data for the Congo-São Francisco (CSF) craton during the Nuna cycle is scarce, and the location of CSF craton has consequently been poorly constrained. Initial models of Nuna placed the CSF craton, together with Amazonia, West Africa, and perhaps Río de la Plata cratons, as part of the Atlantica continent and separate from other parts of Nuna (Rogers, 1996; Rogers and Santosh, 2009) (Fig. 1a); and this was later tested by Elming et al. (2021). Rogers (1996) proposed that Atlantica persisted for more than 1 billion years, until the formation of Gondwana at ca. 600–520 Ma and further until Pangea. Subsequently, however, Atlantica in its original configuration was challenged by Paleoproterozoic paleomagnetic data obtained mainly from Amazonia (+West Africa) and Río de la Plata cratons (D'Agrella-Filho et al., 2011; Rapalini et al., 2015), resulting in a proposed modified configuration and possible connection (Rapalini et al., 2015; Franceschinis et al., 2019).

Based mainly on geological evidence and temporal "barcode" matches of large igneous provinces (Bleeker and Ernst, 2006), and also using sporadic paleomagnetic data, the CSF craton has been reconstructed with other cratons during the Nuna cycle. A connection with Siberian craton was proposed based on barcode matching at ca. 1500 and ca. 1380 Ma by Ernst et al. (2013), but paleomagnetic support for such a reconstruction was limited to an old result (Piper, 1974) that requires confirmation by more modern methods and field tests on the age of remanence acquisition. Pisarevsky et al. (2014), nevertheless, used this relative configuration of CSF and Siberian cratons in their 1500 Ma Nuna reconstruction (Fig. 1c), which at the time was lacking paleomagnetic data for CSF craton. Salminen et al., (2016a) provided a high-quality 1500 Ma Curaça paleomagnetic pole for São Francisco and used this to reconstruct CSF craton in close proximity with Baltica and

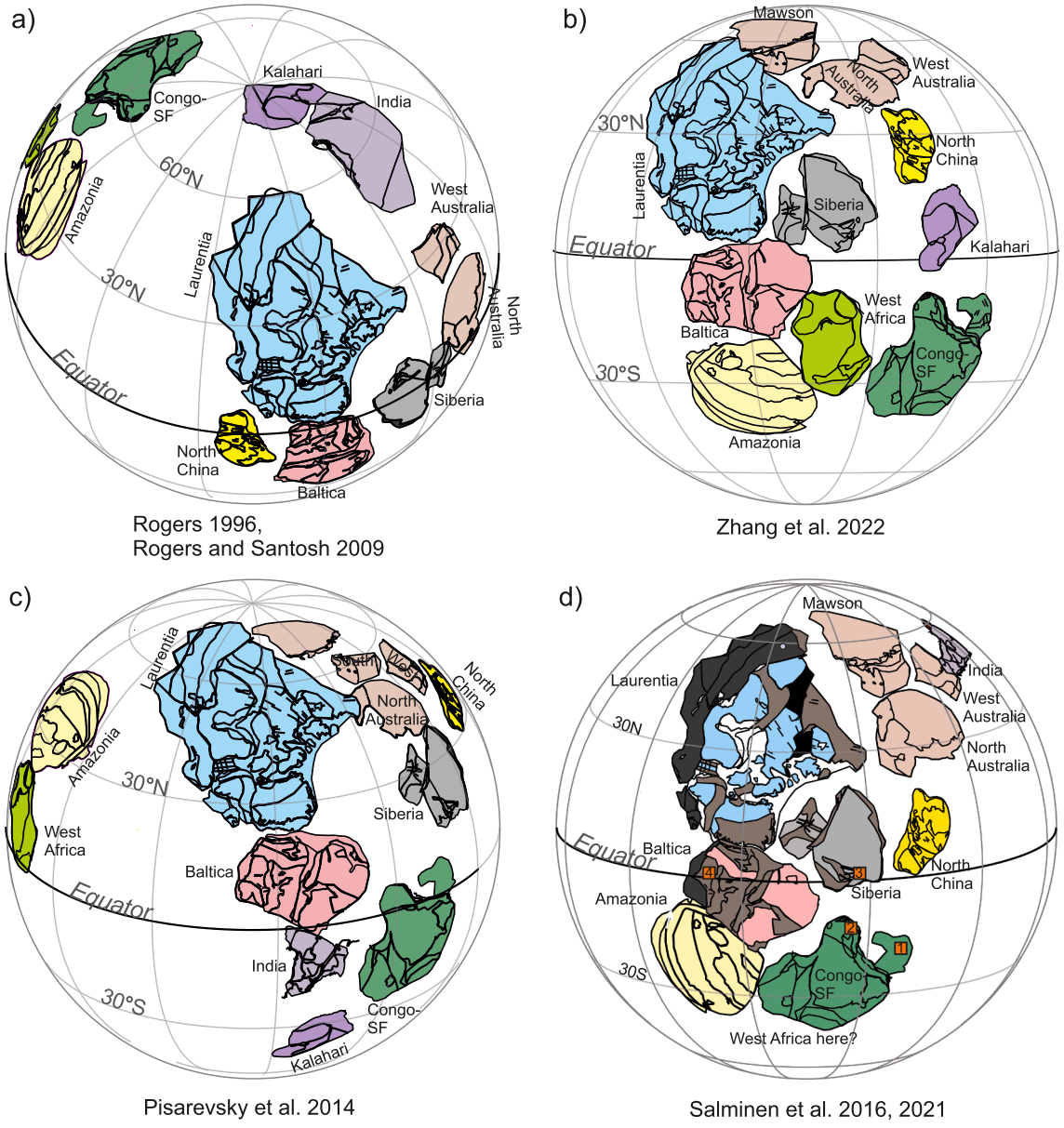

Fig. 1. Selected previous models of Nuna (a) at 1500 Ma after Rogers (1996) and Rogers and Santosh (2009), (b) at 1400 Ma Zhang et al. (2022), (c) at 1500 Ma Pisarevsky et al. (2014), and (d) at 1500 Ma Salminen et al., (2016a); Salminen et al. (2021) (orange squares indicate large igneous provinces, see Fig. 13a). (For interpretation of the references to color in this figure legend, the reader is referred to the web version of this article.)

Siberia (Fig. 1d), and this was later followed by a broadly similar reconstruction model by Zhang et al. (2022) (Fig. 1b). Zhang et al. (2022) also proposed a connection of CSF craton with West African craton (Fig. 1b) based on matching the magmatic barcode at 1380 Ma.

Testing the kinematics of CSF during the Nuna interval is hampered by the sparseness of paleomagnetic data. Only a small number of paleomagnetic data exist for CSF craton (see summary in Salminen et al., 2016a; Trindade et al., 2021), and the only high-quality published pole for the Nuna interval is the 1500 Ma Curaça pole (Salminen et al., 2016a). The motivation for the present study was to obtain geochronological and paleomagnetic data from the 1385 Ma Virei dyke swarm of the Congo craton and to examine the CSF craton's placement within the Nuna cycle

2. Geology and sampling of the Virei mafic dyke swarm

2.1. Geologic overview

Congo and São Francisco cratons are composed of several Archean and Paleoproterozoic nuclei welded together by Paleoproterozoic belts (Hanson, 2003; De Waele et al., 2008; Weber et al., 2016; Trindade et al., 2021) (Fig. 2). This pre-Atlantic assembly of the CSF craton dates back to at least ca. 2000 Ma, with the closure of major Paleoproterozoic orogenic belts related to Nuna amalgamation (e.g., Zhao et al., 2004). The main Archean and Paleoproterozoic nuclei of the Congo craton are the Angola-Kasai block, the NE-Congo-Uganda Block, Bangweulu Block, the Ntem Gabon Block, and the Tanzania craton (de Wit et al., 2015) (Fig. 2). Particularly prominent is the age match of ca. 2000 Ma basement rocks in Bahia (São Francisco craton) and Gabon (Congo craton) (Hurley et al., 1967; Torquato and Cordani, 1981; Porada, 1989). In addition, widespread mafic LIP magmatism with U-Pb baddeleyite ages of 1500 and 920 Ma is found on both continents, further corroborating this *trans*-Atlantic correlations through the barcode comparison (Ernst et al., 2013). Magmatic events at 1380 and 1100 Ma are only reported for Congo craton (not yet found in the São Francisco craton), and instead have been correlated with coeval events in Kalahari craton (e.g., Ernst et al., 2013; Salminen et al., 2018).

The crystalline basement on Angola-Kasai block was intruded during the Mesoproterozoic by a set of mafic sills and dykes of about 1500 and 1100 Ma (Ernst et al., 2013; Salminen et al., 2018), and by the large ca. 1440–1375 Ma Kunene Complex (1438–1375 Ma; e.g., Mayer et al., 2004; Drüppel et al., 2007; Bybee et al., 2019), for which the most recent geochronological results imply more narrower age range at ca. 1384–1375 Ma (U-Pb zircon/baddeleyite ages, Bybee et al., 2019). The WNW-trending mafic Virei dyke swarm trends prominently towards the Mesoproterozoic Kunene Complex but has not been observed to cut it (Fig. 3).

2.2. Sampling of the Virei mafic dyke swarm

Thirty-two WNW-trending mafic dykes were sampled in the southern part of the Congo craton in Angola (Fig. 3) during two field seasons in 2016 and 2018, as a part of a broader study on numerous dyke swarms exposed in the area. Twelve of the sampled dykes yielded usable paleomagnetic results. Wherever the contact between dyke and host rock was visible, the dyke was observed to have a vertical to subvertical dip. Samples for paleomagnetic analyses were taken with a portable field drill. Eight to twelve oriented 2.5 cm diameter core samples were collected from each dyke (interpreted as a separate cooling unit). Baked and unbaked host granite and granitic gneiss at four sites (S1626, S1807, S1812, and S1823) were sampled for baked contact tests. In addition, one crosscutting ENE trending dyke (site S1616) was sampled for an inverse baked contact test. Eighteen to twenty-seven samples were collected from each baked contact test site. Cored samples were oriented using both solar and magnetic compasses. Possible effects of lightning strikes on outcrops were screened for with a magnetic compass. A block

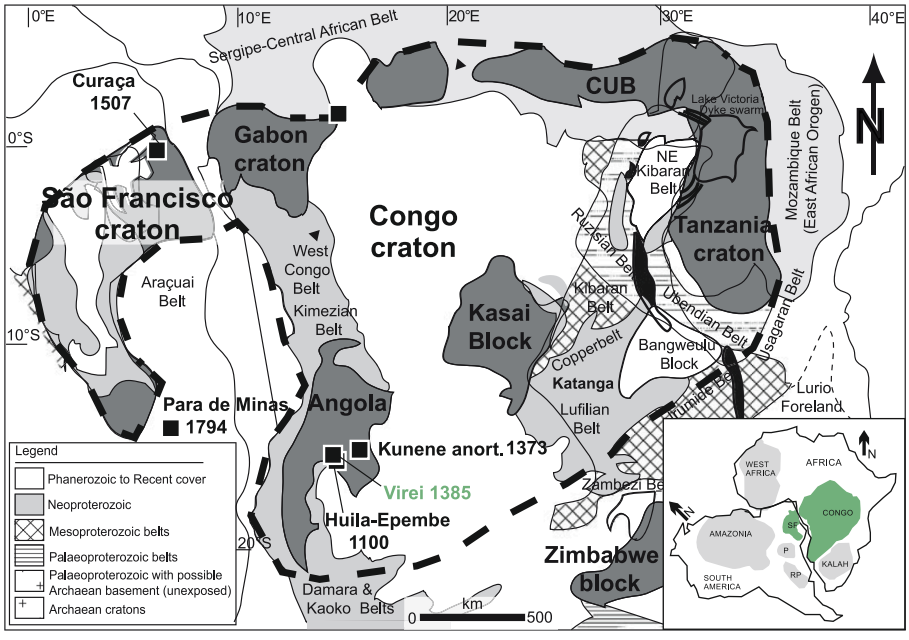

Fig. 2. Regional tectonic map of São Francisco and Congo cratons in a pre-Atlantic configuration. Sites for paleomagnetic poles discussed in this paper are indicated with black squares, where numbers are ages in Ma. ~ 1370 Ma circumferential Lake Victoria dyke swarm indicated (Mäkitie et al., 2014). Inset: cratons of western Gondwana include Kalah – Kalahari, P – Paranapanema, RP – Río de la Plata, SF – São Francisco. Modified from Trindade et al. (2021).

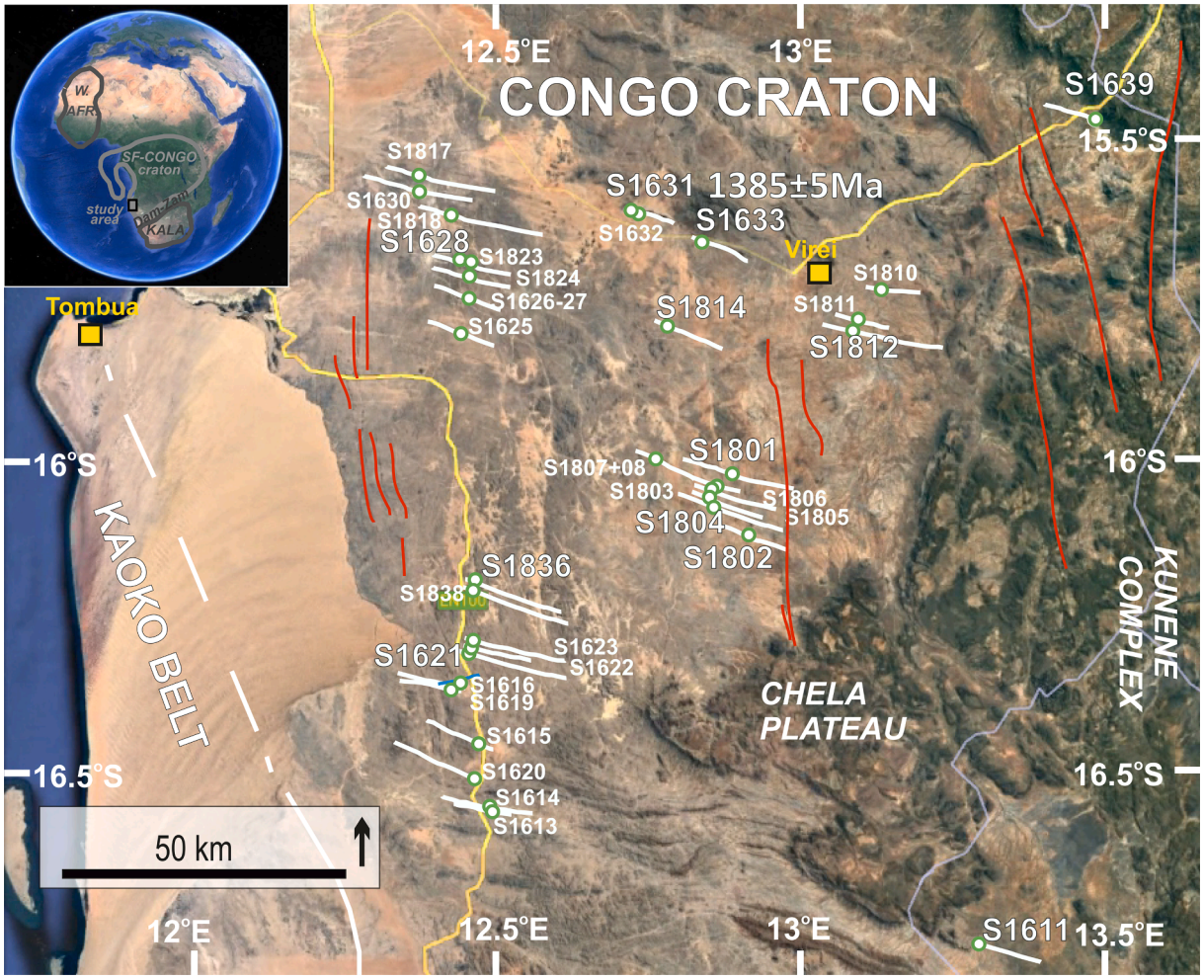

Fig. 3. Site locality map with Google Earth™ background. White lines indicate sampled WNW-trending dykes, from these 12 sites, marked in bold white font with black outlines, yielded acceptable paleomagnetic results. Blue line at site S1616 indicates the crosscutting ENE dyke. Red lines indicate 1.1 Ga dykes (Salminen et al., 2018). Eastern limit of Kaoko belt allochthon is from Goscombe et al. (2018). Inset abbreviations: DLZO–Damara-Lufilian-Zambezi orogen, Kala–Kalahari craton, SF–São Francisco craton, W.Afr.–West African craton. U-Pb baddeleyite age site (S1633) indicated (Lat: 15.6776°S, Long: 12.8075°E). (For interpretation of the references to color in this figure legend, the reader is referred to the web version of this article.)

sample was taken from a 50 m wide dyke (S1633) close to the town of Virei (Lat: 15.6776°S, Long: 12.8075°E), for geochronology (Fig. 3). In addition, block samples were collected for geochemical analyses from all dykes that were sampled for paleomagnetic study few hundred meters away from paleomagnetic sampling site .

3. Methods

3.1. Geochronological methods

Baddeleyite was separated from dyke S1633, a coarse-grained dyke close to Virei (Fig. 3), using the water-based separation technique of Söderlund and Johansson (2002) at the Department of Geology, Lund University. About 40 dark brown baddeleyite grains were recovered. The best grains were combined into three fractions comprising 5–7 grains in each. The U and Pb isotopic compositions were measured at the Department of Geosciences at the Swedish Museum of Natural History using a Thermo Scientific - Finnigan TRITON isotope dilution thermal ionization mass spectrometer (ID-TIMS). The U and Pb isotopic compositions of the samples were measured in dynamic (peak jumping) mode using a secondary electron multiplier. The procedural blank in the isotope laboratory at the Swedish Museum of Natural History was determined to be 0.8 pg for Pb and 0.08 pg for U. Mass fractionation for Pb was determined by replicate analyses of the common and radiogenic NIST standard reference materials SRM 981 and SRM 983. U fractionation was obtained directly from the measured $^{233}U/^{236}U$ isotopic ratio (close to unity). The Stacey and Kramers (1975) common Pb evolution curve was used to estimate initial Pb compositions in each fraction measured. The decay constants used were 1.55125×10^{-11} (^{238}U) and 9.8485×10^{-10} (^{235}U), with the isotopic composition of U being $^{238}U/^{235}U = 137.88$ (Jaffey et al., 1971; Steiger and Jäger, 1977). The final analytical results were calculated and plotted using the Microsoft Excel Macro, Isoplot (Ludwig, 2003).

3.2. Geochemical methods

Twelve bulk rock samples were processed and analysed for major and trace elements at Stellenbosch University's Central Analytical Facility, as specified in greater detail by Klausen et al. (2017). Samples were first cleaned, and then fresh blocks were cut for steel jaw crushing. A small handful of quarter-and-cone split crushed sample material was milled in a tungsten-carbide swing mill with a Co-binder in its lining. Sample millings were intermingled with clean quartz runs. Powders were fused into La-free glass beads for both (1) major element X-Ray Fluorescence (XRF) analysis using Philip's PW1404w instrument (Axios from PANalytical with a 2.4 kWatt Rh X-ray Tube), and (2) trace element analysis, using an Agilent 7500ce ICP-MS coupled with a Nd-YAG 223 nm New Wave LASER ablation (LA) system operating at a 12 Hz

Table 1
U-Pb TIMS data of the sample from the Virei swarm, Angola, corresponding to paleomagnetic site S1633.

Analysis no. (number of grains)	U/Th	Pb_c/Pb_{tot}[1]	$^{206}Pb/^{204}Pb$	$^{207}Pb/^{235}U$	±2σ %err	$^{206}Pb/^{238}U$	±2σ %err	$^{207}Pb/^{235}U$	$^{206}Pb/^{238}U$	$^{207}Pb/^{206}Pb$	±2σ	Concordance
			raw[2]		[corr][3]				[age, Ma]			
Bd-1 (6 grains)	n.m.	0.110	610.1	2.8619	1.32	0.23586	1.3	1371.9	1365.2	1382.5	8.7	0.987
Bd-2 (5 grains)	n.m.	0.046	1021.3	2.8802	0.97	0.23684	0.94	1376.7	1370.3	1386.8	6.8	0.988
Bd-3 (7 grains)	n.m.	0.098	567.2	2.7652	2.16	0.22791	2.12	1346.2	1323.5	1382.4	11.4	0.957

[1] Pbc = common Pb; Pbtot = total Pb (radiogenic + blank + initial): n.m. = not measured.
[2] Measured ratio, corrected for fractionation and spike.
[3] Isotopic ratios corrected for fractionation (0.1 % per amu for Pb), spike contribution, blank (0.8 pg Pb and 0.08 pg U), and initial common Pb. Initial common Pb corrected with isotopic compositions from the model od Stacey and Kramers (1975) at the age of the sample.

Table 2
Bulk rock geochemistry of the Virei swarm, Angola.

Sample	S1633	S1611	S1621	S1628	S1801	S1802	S1802M	S1804	S1812	S1814	S1836	S1811
Latitude	−15.6707	−16.7407	−16.3400	−15.7158	−16.0271	−16.1198	−16.1198	−16.0577	−15.8037	−15.7999	−16.2078	−15.7984
Longitude	12.7910	13.2420	12.4373	12.4292	12.8557	12.8809	12.8809	12.8170	13.0450	12.7487	12.4445	13.0509
Major oxides and LOI (wt%)												
SiO_2	46.20	46.80	49.66	42.90	45.27	43.58	43.52	42.04	48.82	47.60	44.96	44.03
TiO_2	0.64	1.60	1.72	4.04	1.63	2.78	3.02	3.04	1.70	3.63	3.39	4.00
Al_2O_3	19.96	16.69	13.90	14.19	17.09	15.66	15.21	15.95	17.99	13.94	15.62	14.26
Fe_2O_3	10.46	13.24	13.42	18.02	12.93	15.82	15.97	16.81	12.27	16.45	16.97	17.28
CaO	9.64	8.57	10.13	7.22	8.66	9.12	8.40	6.66	5.12	7.10	7.34	7.03
MgO	10.05	6.57	6.24	4.99	7.25	6.65	6.65	5.35	3.65	4.20	5.53	4.76
MnO	0.14	0.19	0.22	0.23	0.18	0.20	0.24	0.22	0.16	0.22	0.20	0.20
Na_2O	2.39	2.29	1.94	3.29	2.13	2.04	2.83	3.00	5.20	3.01	2.94	3.02
K_2O	0.23	1.28	0.67	1.84	0.95	0.93	0.74	2.55	0.56	1.86	1.19	1.43
P_2O_5	0.13	0.41	0.18	1.26	0.22	0.76	0.83	0.84	0.24	1.09	0.91	1.12
LOI	0.18	2.15	0.96	1.10	3.92	3.35	3.35	4.18	5.71	1.45	1.36	3.26
Total	100.02	99.83	99.04	99.08	100.24	100.90	100.77	100.65	101.43	100.55	100.42	100.39
Trace elements (ppm)												
Sc	13.56	27.30	42.00	24.80	29.71	24.52	26.78	27.04	31.03	28.10	26.37	25.69
V	79.5	212.5	316.0	200.1	255.8	252.4	258.8	255.1	271.9	240.8	254.9	240.0
Cr	56.6	67.2	53.1	13.4	115.1	82.4	81.4	85.4	124.8	26.7	59.9	30.5
Ni	201.1	93.6	71.4	52.6	137.4	94.3	83.8	91.9	137.0	35.1	75.5	48.5
Cu	31.2	58.5	98.4	61.5	59.8	54.7	51.2	28.3	88.1	44.9	57.1	52.5
Zn	132.3	110.2	105.1	145.8	103.2	123.3	171.6	193.7	184.5	150.8	159.9	152.3
Rb	3.42	50.40	17.54	39.20	37.80	29.93	22.08	89.20	26.14	39.38	23.95	33.63
Sr	406	523	243	344	336	414	280	333	237	375	402	356
Y	6.91	26.47	23.66	47.22	21.66	29.68	32.28	32.82	23.28	45.96	41.71	41.73
Zr	33.2	120.1	98.3	326.5	103.6	150.7	167.6	167.7	117.9	334.8	276.8	303.7
Nb	3.07	7.23	5.74	20.91	7.57	12.94	14.24	14.55	8.45	23.37	20.24	22.86
Mo	0.190	0.340	0.420	1.080	0.570	0.910	1.145	0.575	0.655	1.510	0.975	1.495
Cs	0.372	11.035	0.795	1.985	0.850	2.605	3.465	7.285	2.245	3.075	0.421	1.845
Ba	130	543	516	757	831	574	627	1328	176	1084	637	735
La	4.61	23.41	10.05	42.19	12.72	22.13	23.64	23.84	14.66	46.92	34.01	40.71
Ce	10.27	51.60	23.07	96.30	27.34	50.65	55.04	56.08	31.69	102.75	77.00	91.20
Pr	1.31	6.56	3.23	12.62	3.66	6.83	7.44	7.58	4.15	13.29	10.14	11.90
Nd	6.12	28.70	15.04	57.05	17.28	31.44	33.39	34.75	19.02	58.61	45.75	52.75
Sm	1.34	5.85	3.64	12.10	4.03	7.04	7.48	7.82	4.33	12.06	10.02	10.82
Eu	0.676	1.665	1.255	3.210	1.396	2.285	2.411	2.549	1.176	3.420	2.965	3.215
Gd	1.43	5.72	4.55	11.34	4.59	6.80	7.44	7.56	5.00	11.24	9.74	10.02
Tb	0.223	0.829	0.716	1.505	0.664	0.950	1.069	1.096	0.726	1.540	1.392	1.414
Dy	1.33	5.39	4.65	9.13	4.28	6.11	6.74	6.74	4.71	9.36	8.70	8.60
Ho	0.250	1.003	0.937	1.782	0.873	1.195	1.279	1.326	0.972	1.764	1.690	1.647
Er	0.670	3.105	2.520	4.825	2.535	3.325	3.560	3.755	2.660	5.085	4.750	4.590
Tm	0.089	0.380	0.369	0.617	0.344	0.439	0.494	0.477	0.385	0.684	0.633	0.617
Yb	0.510	2.665	2.340	4.265	2.280	2.895	3.200	3.205	2.465	4.340	4.345	4.040
Lu	0.091	0.400	0.354	0.615	0.318	0.422	0.447	0.453	0.356	0.632	0.614	0.586
Hf	0.85	3.17	2.77	7.68	2.95	4.09	4.51	4.62	3.25	8.25	7.06	7.45
Ta	0.146	0.330	0.328	1.152	0.417	0.747	0.796	0.819	0.472	1.236	1.080	1.265
Pb	1.22	6.29	12.51	7.88	3.60	3.73	6.40	62.00	286.80	11.01	5.54	8.53
Th	0.381	1.309	1.362	1.623	1.171	1.467	1.418	1.446	1.494	4.325	2.542	3.505
U	0.065	0.308	0.391	0.437	0.193	0.318	0.323	0.372	0.304	0.960	0.538	0.788

LOI - loss of ignition

frequency with a mixed He-Ar carrier gas (following method by Eggins, 2003). A wide range of international (NIST®) and national (SARM®) standards (Pearce, 1996) were analysed concurrently with the samples.

3.3. Rock magnetic methods

Magnetic mineralogies of the samples from each dyke site were investigated by thermomagnetic bulk susceptibility analyses of the powdered whole-rock samples. The volume of the analyzed material ranged between 0.5 and 1 cm^3. Temperature dependence of low-field magnetic susceptibility was measured from 20 °C to ~ 700 °C in argon atmosphere followed by cooling back to room temperature for the year-2016 samples at the University of Helsinki using AGICO KLY-3S kappabridge (field intensity 300 A/m, frequency 875 Hz) and for the year-2018 samples at the Geophysical Laboratory of the Geological Survey of Finland using the AGICO MFK1-FA Kappabridge (field 350 A/m, frequency 976 Hz). Data processing and correction for empty furnace susceptibility were done using the Cureval 8.0.2-software (Chadima and Hrouda, 2012).

3.4. Paleomagnetic methods

The paleomagnetic cores were cut into specimens in the laboratory at Yale University using a non-magnetic dual blade saw. Specimens for paleomagnetic analyses were split into two parts, which were measured in the magnetically shielded room of the paleomagnetic laboratory at the Department of Geology and Geophysics (now Earth and Planetary Sciences) at Yale University (USA) and in the Solid Earth Geophysics Laboratory at the University of Helsinki (Finland). At Yale University, after the measurement of natural remanent magnetization (NRM), the samples were immersed in liquid nitrogen in magnetically shielded room in order to reduce a viscous component carried by larger magnetite grains (Schmidt, 1993). The samples were then thermally demagnetized using a nitrogen-atmosphere ASC Scientific model TD-48SC furnace. After each step the remanent magnetization was measured using an automated sample-changing system attached to a 2G (now WSGI) cryogenic magnetometer (Kirschvink et al., 2008). At the University of Helsinki, samples were demagnetized either using the in-line static 3-axis alternating field (AF) system paired to the 2G cryogenic magnetometer or using an argon-atmosphere ASC Scientific model TD-48SC furnace. In both laboratories, demagnetization was continued until the magnetic intensity of the specimens dropped below system noise level or until the measured directions became erratic and unstable. Both the thermal and AF (for most of the samples) methods were effective and results from both laboratories are comparable. Vector components were isolated using principal component analysis (Kirschvink, 1980; Jones, 2002). We employed the standard convention of assigning "normal" polarity to N-up ChRM vectors from Proterozoic rocks in the Congo craton. The maximum angle of deviation (MAD) (Kirschvink, 1980) was less than 11° for the accepted specimens. The mean directions were calculated using Fisher statistics (Fisher, 1953) by giving unit weight to each sample; in cases of two (three) specimens per sample, each specimen was assigned 0.5 (0.333) weight. Acceptable sites consisted of a minimum of five separate samples showing similar directions. For calculating the paleomagnetic pole, we applied the constant cutoff angle of 45°, which is commonly used to exclude transitional virtual geomagnetic poles (VGPs) (e.g., Johnson et al., 2008). The maximum deviation of a VGP from the mean paleopole was 42°.

The site-dependent paleosecular variation (PSV) test of Deenen et al. (2011) was used to explore if virtual geomagnetic poles average the secular variation (Table 3). A reversal test was conducted on the normal and reversed polarity groups (McFadden and Lowes, 1981; McFadden and McElhinny, 1990) using super-IAPD (Torsvik et al., 2000) program and using the test of Heslop and Roberts (2018) for the common mean. Paleogeographic reconstructions and pole plots used the GPlates software (Müller et al., 2019).

4. Results

4.1. Geochronological results

The three baddeleyite fractions analyzed from the dyke S1633 (Table 1) form a cluster just below the concordia curve (Fig. 4). The three fractions yield upper and lower intercept dates of 1387 ± 9 Ma and 149 ± 510 Ma, respectively. Concordance varies between ~96 % and ~98 %, with the most concordant baddeleyite date having a $^{207}Pb/^{206}Pb$ date of 1386.8 ± 6.8 Ma (2σ). Since two of the three fractions marginally overlap the concordia curve, we prefer using the weighted mean of $^{207}Pb/^{206}Pb$ dates of the analyses. This yields an age of 1385 ± 5 Ma (MSWD = 0.39), which is almost identical and well within error of the

Table 3
Paleomagnetic data of the Virei swarm, Angola.

Site	Lat (°)	Lon (°)	Pol	D (°)	I (°)	k	a95 (°)	Plat (°)	Plon (°)	K	A95 (°)	B	N	n
S1628	−15.7085	12.4123	N	6.6	−37.6	22.2	16.6	80.4	147.1	26.9	15.0	1	5	5
S1639	−15.4827	13.4268	N	345.1	−52.4	35.9	11.3	67.0	226.3	43.6	10.3	1	6	6
S1802	−16.1198	12.8809	N	293.0	−48.6	40.3	10.7	27.4	256.9	32.4	11.9	1	6	9
S1804	−16.0577	12.8170	N	302.2	−78.7	61.1	11.8	26.6	212.8	18.7	21.8	1	4	5
S1814	−15.7999	12.7487	N	334.6	−43.5	19.6	15.5	63.7	251.9	24.6	13.8	1	6	6
Mean N-polarity	−15.8337	12.8571	N	334.3	−55.2	11.6	23.5	57.0	234.6	7.2	30.6	5	27	31
S1611	−16.7407	13.2420	R	112.9	35.4	16.8	16.8	26.6	269.3	24.7	13.7	1	6	9
S1621	−16.3399	12.4375	R	143.0	56.1	15.0	20.4	51.5	243.3	8.6	27.6	1	5	6
S1631	−15.6302	12.6967	R	316.5	79.1	79.1	7.6	0.0	178.4	26.3	13.3	1	6	13
S1633 (1385 Ma)	−15.6743	12.7952	R	93.8	33.4	61.1	7.8	8.3	266.1	64.5	7.6	1	7	10
S1801	−16.0271	12.8557	R	73.3	44.0	19.1	17.9	−7.4	253.3	26.3	15.2	1	5	7
S1812	−15.8037	13.0450	R	70.2	69.9	72.5	7.1	1.6	226.8	29.6	11.3	1	7	8
S1836	−16.2078	12.4445	R	169.4	55.6	57.0	8.1	67.9	215.8	28.9	11.4	1	7	7
Mean R-polarity	−16.0605	12.7881	R	107.4	60.6	7.5	23.6	23.6	238.6	4.0	34.5	7	43	60
Mean N + R	**−15.9660**	**12.8168**	**N + R**	**309.2**	**−60.4**	**7.9**	**16.5**	**38.5**	**237.3**	**4.5**	**23.2**	**12**	**70**	**91**
													A95 max	**A95 min**
													17.1	**4.4**
Excluded from mean														
S1807*	−16.0078	12.7307	R	288.0	41.3	523.2	3.3	−9.3	130.8	393.0	3.9	1	5	5
S1811*	−15.7984	13.0509	R	225.2	43.0	9.2	23.3	46.8	123.0	9.3	23.2	1	6	8

Slat/Slong, Latitude/longitude of sampling site. Pol., polarity of the isolated magnetization direction: N/R, normal/reversed polarity. D, declination. I, inclination. k, precision parameter for directions. a95, the radius of the 95 % confidence cone in Fisher (1953) statistics. Plat/Plong, paleolatitude/paleolongitude of the pole. K, precision parameter for poles. A95, radius of the 95 %. A95max and A95 min after Deenen et al., 2011. B/N/n, number of sites/samples/specimens. *excluded from mean.

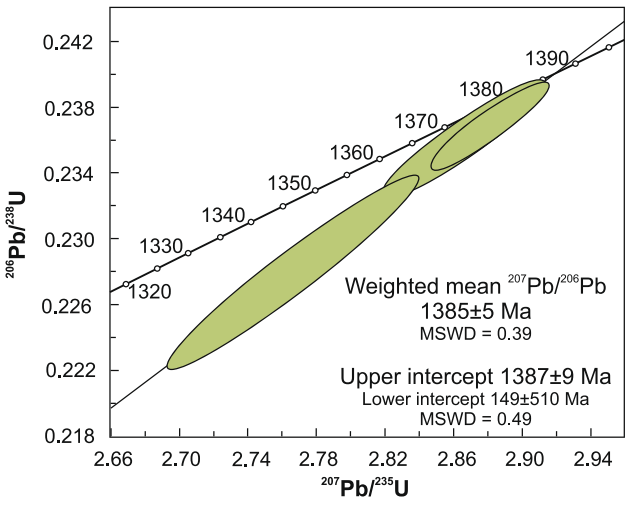

Fig. 4. Wetherill U-Pb isotope diagram for the analyzed baddeleyite fractions of dyke S1633 in Angola, with uncertainties of individual fractions given at 2σ-level. MSWD—mean square of weighted deviates.

upper intercept date. Considering the minor discordance, we prefer to report this more precise result as the best age estimate of the intrusion.

4.2. Bulk rock geochemistry

Bulk rock geochemistry was made for eleven dykes (Table 2), including the dated dyke S1633. Both a margin (S1802M) and core (S1802) sample were analysed for one dyke, recording minimal internal compositional variation. Analysed samples show a large scatter in total alkalies and silica ($Na_2O + K_2O$ and SiO_2, respectively, in Fig. 5a), ranging from most alkali tephrites to tholeiitic basalts, as well as one basaltic trachy-andesite. In contrast all twelve samples cluster as non-alkali basalts within Pearce's (1996) classification diagram (Fig. 5b), defined by high field strength element ratios that are more robust against the mobilization by hydrothermal fluids and metamorphism than alkalies and silica.

Seven samples from the more alkali dykes are overall slightly more enriched in incompatible elements, compared with three of the more tholeiitic basalt samples and a basaltic trachy-andesite (red versus purple colors, respectively, in Fig. 6a) and these groups will correspondingly be referred to as "alkali" and "tholeiitic", respectively, even if this distinction may be subtle. While the ~ 1385 Ma dated dyke (S1633) plots as a tholetiitic basalt, it also exhibits overall abnormally low concentrations of most incompatible elements, explained by the

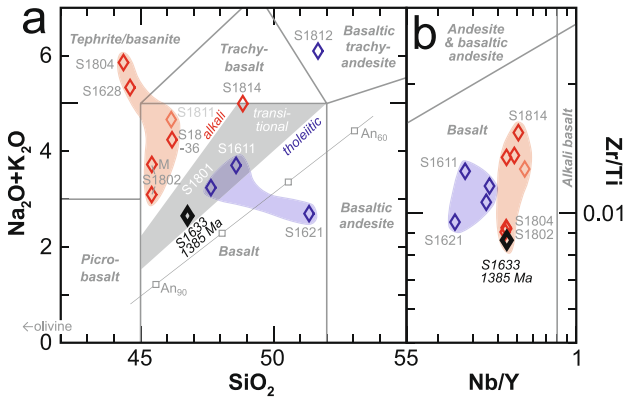

Fig. 5. Geochemical classification of ~ 1385 Ma Virei dykes. (a) TAS-diagram by Le Maitre et al. (2002). (b) Incompatible element ratio plot by Pearce (1996). Color-coding as explained in the text.

accumulation of observed, euhedral and incompatible element-poor olivines and plagioclases within this sample, which would have expelled an incompatible element rich intercumulus melt. Despite this physical lowering of incompatible element concentrations, their pattern for S1633 still compares remarkably well with those by other samples, as shown by an elevated grey copy of this pattern in Fig. 6a, excluding Sr and Eu. Such parallelism between incompatible element patterns argues for all dykes being part of the same ~ 1385 Ma swarm, even if slight differences in incompatible signature (pattern and ratios) between alkali and tholeiitic dykes is more consistent with belonging to separate subswarms.

In more detail, petrogenetic plots in Fig. 6(b-c) further imply that alkali dykes, including the dated S1633, are more 'asthenospheric', while tholeiitic dykes incorporated a slightly greater lithospheric component, either through crustal assimilation and/or the interaction of a subduction-zone-modified sub-continental lithospheric mantle (SZLM by Pearce et al., 2021). While the dated S1633 dyke, with 'tholeiitic' major element signatures, could have acquired its conflicting 'alkali' incompatible element ratios through the accumulation of Ti- and Nb-rich oxides – where Proterozoic massif anorthosites are known for their accumulations of apatite- and ilmenite-rich nelsonites (Ashwal, 1993; Owens and Dymek, 2001) – this is not supported by the presence of cumulus opaques in its thin section.

4.3. Rock magnetic and paleomagnetic results

Representative thermomagnetic curves for samples from selected WNW-trending dyke samples from the Virei dyke swarm are shown in Fig. 7. Heating curves show Curie points in the range of 575–580 °C and Hopkinson's peaks indicating magnetite with low Ti-content (e.g., Dunlop, 2014). In addition, samples from sites S1628, S1639 and S1802 show Curie points at 320 °C pointing to the presence of minor monoclinic pyrrhotite (Dekkers, 1990). Most of the samples show irreversible curves indicating formation of magnetite and occasionally maghemite upon heating; the exception is sample S1804, which shows reversible curves.

Most dyke sites show two components of remanent magnetization (Fig. 8). Twelve of the accepted sites show either a normal polarity NW-up intermediate-steep characteristic remanent magnetization (ChRM) direction (five sites corresponding to five separate cooling units) or a reversed polarity SE-down intermediate-steep ChRM direction (seven sites) (Fig. 9, Table 3). Two dyke sites (S1807, S1811) showing stable ChRM were excluded from the mean based on the chosen 45° cutoff angle (e.g., Johnson et al., 2008). In general, the ChRMs for the accepted twelve sites were obtained with unblocking temperatures up to ca. 500–580 °C and with coercivities varying between 30 and 100 mT, typical for titanomagnetite, which presence was further supported by rock magnetic analyses. The exceptions were the sites S1628 and S1639, for which thermal demagnetization was more effective than AF demagnetization in distinguishing a ChRM component. This is explained by thermomagnetic analyses, which showed the presence of monoclinic pyrrhotite in these sites. Monoclinic pyrrhotite typically has a high coercivity, but its unblocking temperature is ca. 320 °C (Dekkers, 1990). The ChRM directions are defined with a mean angular deviation (MAD) typically less than 5°; but in some cases a MAD as high as 11° was accepted. The reversal test of McFadden and McElhinny (1990) for the chosen twelve sites yields an indeterminate result (obtained angle between the directions: 24.9° and critical angle: 31.1°). The estimated probability for the common mean with the test of Heslop and Roberts (2018) is 0.32 but is an ambiguous result that lends only weak support for a common mean. The mean direction of the twelve accepted site-mean VGPs is at D = 309.2°, I = -60.4° with k = 7.9 and α_{95} = 16.5°. Low- to moderate-temperature and low-coercivity remanent magnetization components for samples were scattered and not coherent enough to produce clustered means for mean calculations.

Attempted baked contact tests for sites S1626, S1807, S1812, and

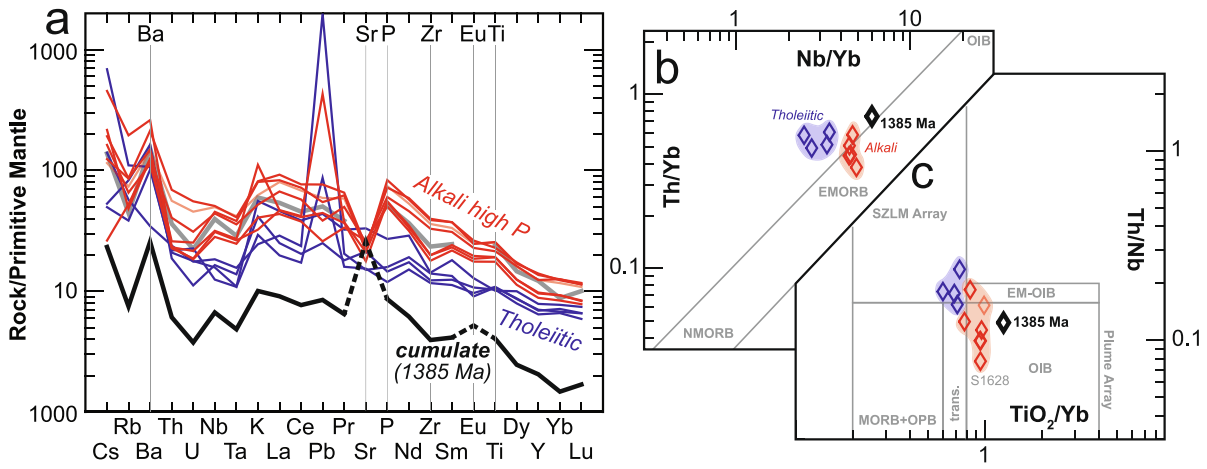

Fig. 6. Geochemical signatures of ~ 1385 Ma Virei dykes. (a) Incompatible element patterns, normalized according to Lyubetskaya and Korenaga (2007). Incompatible element ratio plots by (b) Pearce (2008) and (c) Pearce et al. (2021).

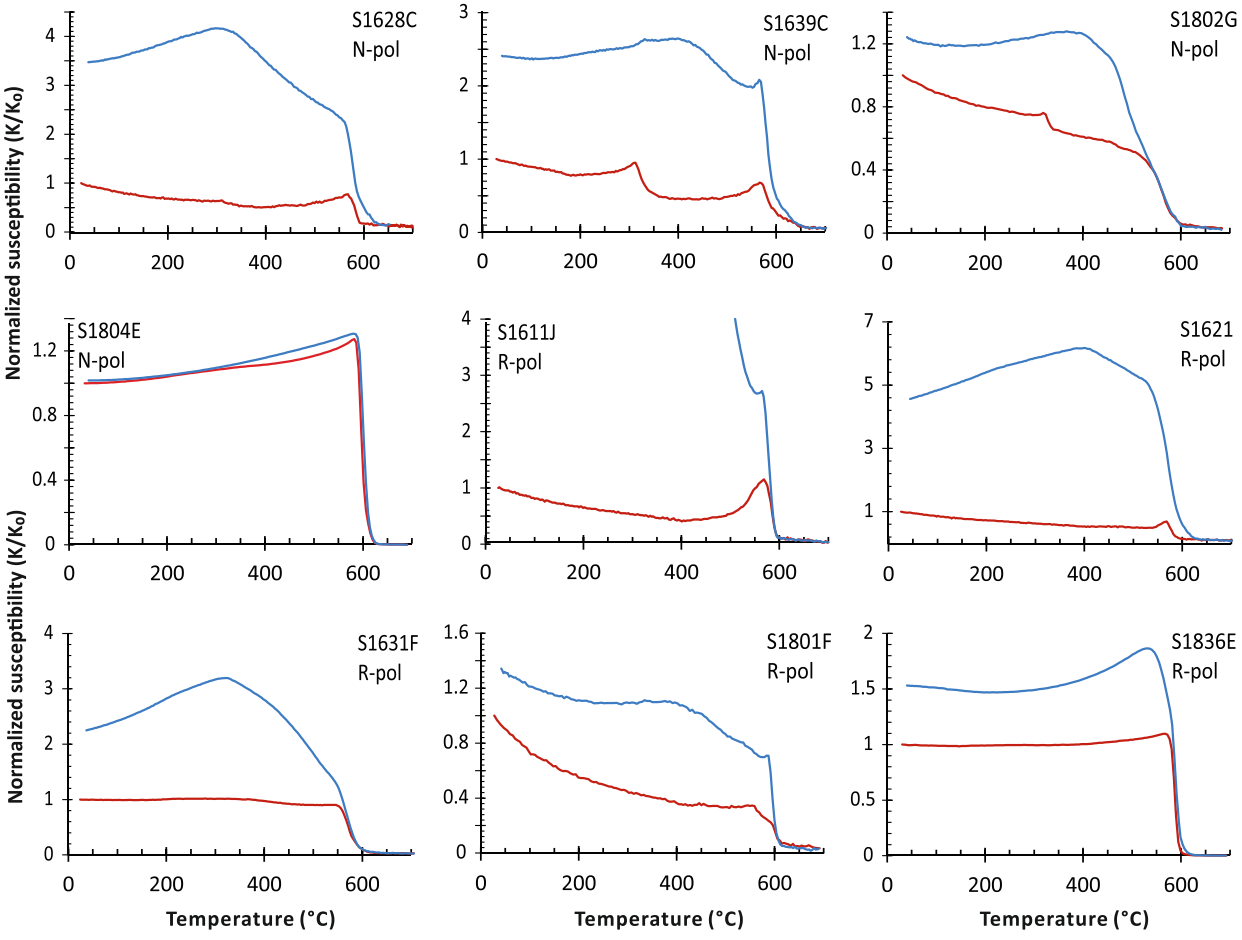

Fig. 7. Normalized susceptibility vs. temperature of the samples from the WNW-trending mafic dyke sites showing either normal polarity (N-pol) or reversed polarity (R-pol) characteristic remanent magnetization directions. Red – heating, Blue – cooling. (For interpretation of the references to color in this figure legend, the reader is referred to the web version of this article.)

S1823 were inconclusive mainly due to scattered ChRM directions in the host rock. In addition, the dyke at baked contact site S1626 shows a presumed Cambrian overprint, and the dyke at site S1823 shows a scattered magnetization direction. One crosscutting ENE dyke at site S1616 was sampled for an inverse baked contact test, but neither the WNW-trending nor the ENE-trending dyke showed stable results at that locality.

Other sampled WNW-trending dykes showed scattered results either due to lightning strike, not being drilled from in situ outcrops, or recording a magnetization direction that could possibly date from regional low-grade metamorphism of Ediacaran-Cambrian age. This possible Cambrian overprint was obtained mainly from the westernmost sites (S1614, S1615, S1626, S1630, S1838) that were sampled more proximal to the Kaoko belt, which is contiguous with the Damara belt

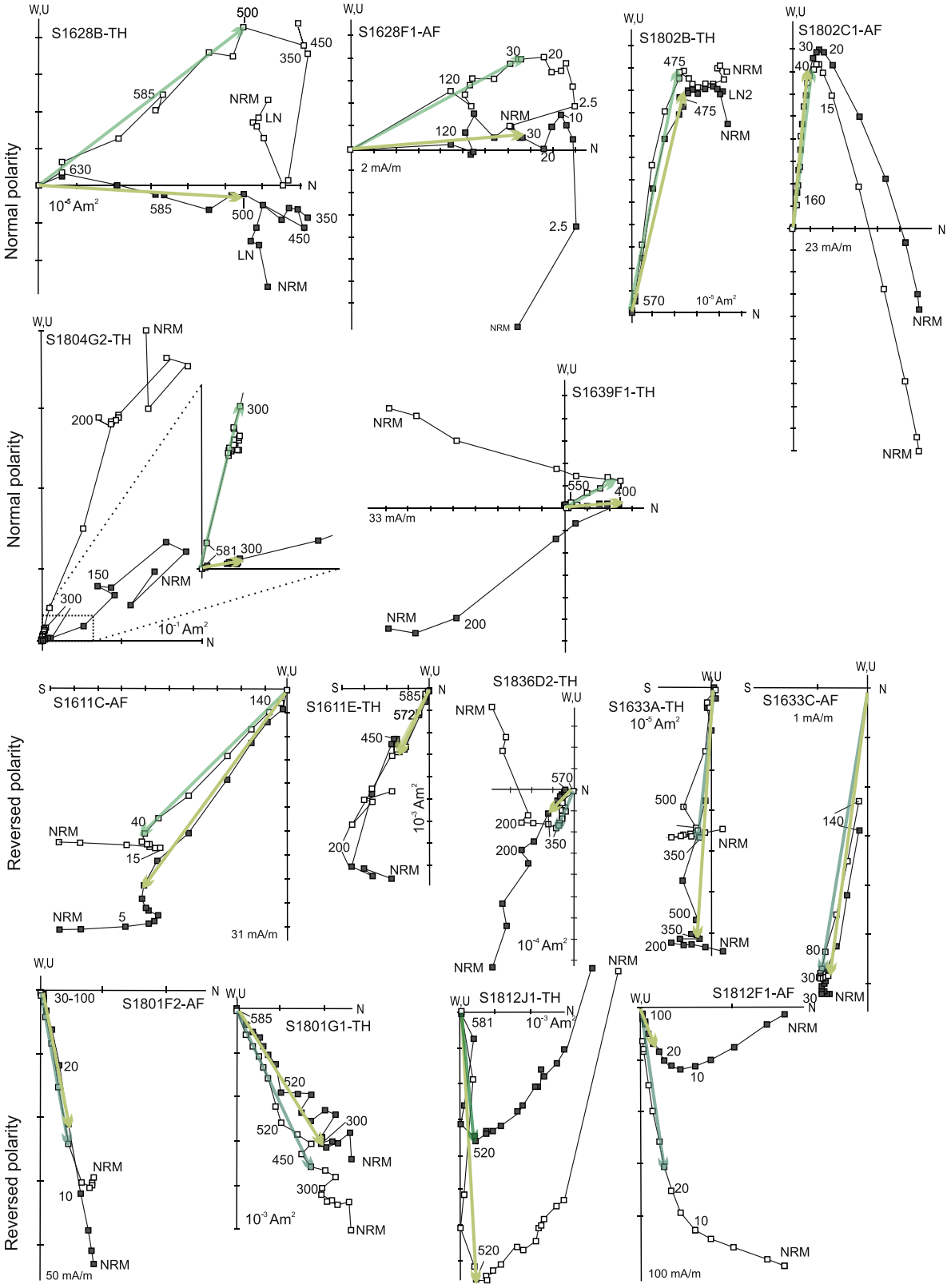

Fig. 8. Zijderveld diagrams and stereographic projection of the thermal and alternating field demagnetization results of representative samples from the dykes of the 1385 Ma Virei swarm. The green arrows indicate the characteristic remanent magnetization direction of each sample. (For interpretation of the references to color in this figure legend, the reader is referred to the web version of this article.)

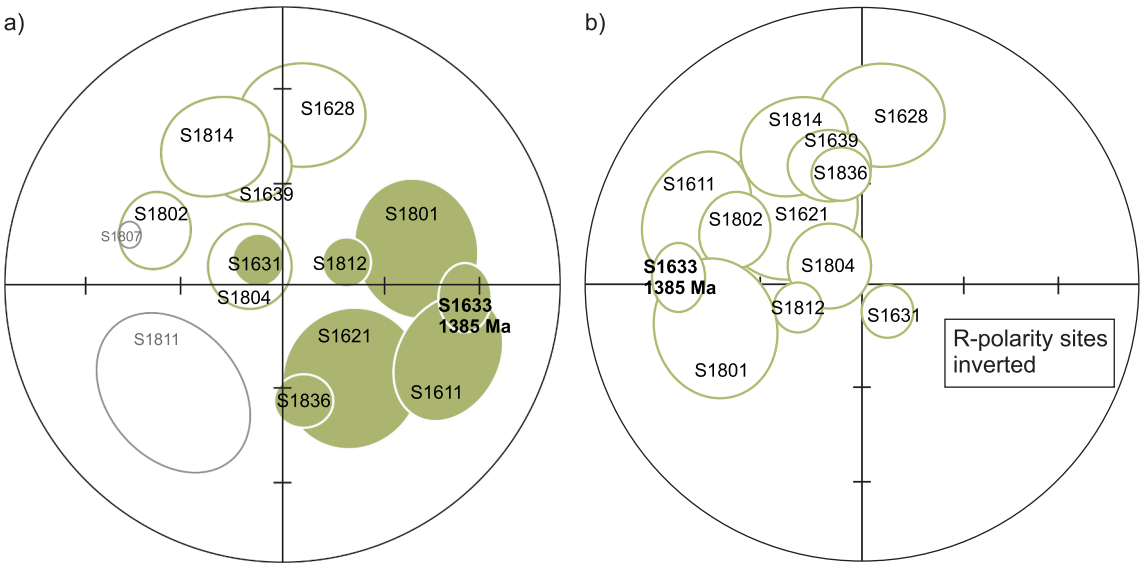

Fig. 9. (a) Stereographic equal-area projection of site mean ChRM directions of 1385 Ma Virei dykes with α95 error circles (Table 3). (b) Data for reversed polarity sites is inverted. Closed (open) symbols represent downward (upward) directions. Dyke at site S1633 is dated. Sites S1807 and S1811 are excluded from the mean (grey, both drections are on the lower hemisphere).

(Goscombe et al., 2018; Fig. 3). Such a well-defined geographic association of a recognizable remagnetization direction suggests that our selected Virei dual-polarity ChRM is older than Ediacaran-Cambrian in age (similar to what was found from the same region by Salminen et al., 2018).

5. Discussion

5.1. *Kunene-Kibaran large igneous province and global magmatic barcode comparison*

Outcrop trends of the mafic dykes of the dated 1385 ± 5 Ma Virei swarm point ESE toward the extensive ca. 1440–1375 Ma (U-Pb) anorthositic Kunene Complex associated with 1450–1360 Ma A-type red granites (e.g., Mayer et al., 2004; Drüppel et al., 2007; Maier et al., 2013; Bybee et al., 2019; Milani et al., 2022; Djeutchou et al., 2024) (Fig. 3). Recent high precision U-Pb geochronology indicates narrower age range of ca. 1384–1375 Ma for the Kunene anorthosites (Bybee et al., 2019). Tack et al. (2010) noted that the emplacement of the anorogenic Kunene Complex is coeval with ca. 1385–1375 Ma compositionally bimodal magmatism (i.e., Kibaran Event), located 1000 km away on the eastern part of the Congo craton, in the Karagwe-Ankole belt. Magmatism in the Karagwe-Ankole belt consists of Kabanga-Musongati mafic and ultramafic layered complexes, and voluminous granitoid rocks with accompanying mafic intrusive rocks. We follow Tack et al. (2010) and Ernst et al. (2013) in suggesting a tectonomagmatic link between the anorogenic Kunene Complex and associated silicic magmatism and the bimodal magmatism at the Karagwe-Ankole belt, as well as the Lake Victoria circumferential swarm (Mäkitie et al., 2014). We propose that these widely distributed suites of mafic–ultramafic and silicic magmatism represent a craton-margin-wide Kunene-Kibaran large igneous province (LIP) (term introduced in Ernst et al., 2013), so that the Virei dyke swarm is part of this ca. 1385–1375 Ma LIP. Recently an age range of ca. 1380–1360 Ma has been assigned to the Kunene-Kibaran LIP (Djeutchou et al., 2024).

With recognition of the ca. 1385–1375 Ma Kunene-Kibaran LIP, the magmatic barcode record of the CSF craton now includes four LIP events for the Nuna cycle (Fig. 10). From these, the ca. 1385–1375 event has so far been recognized only from the Congo portion of the combined craton, the ca. 1500 Ma event has been recognized in both the São Francisco and Congo cratons, and the older events have so far only been

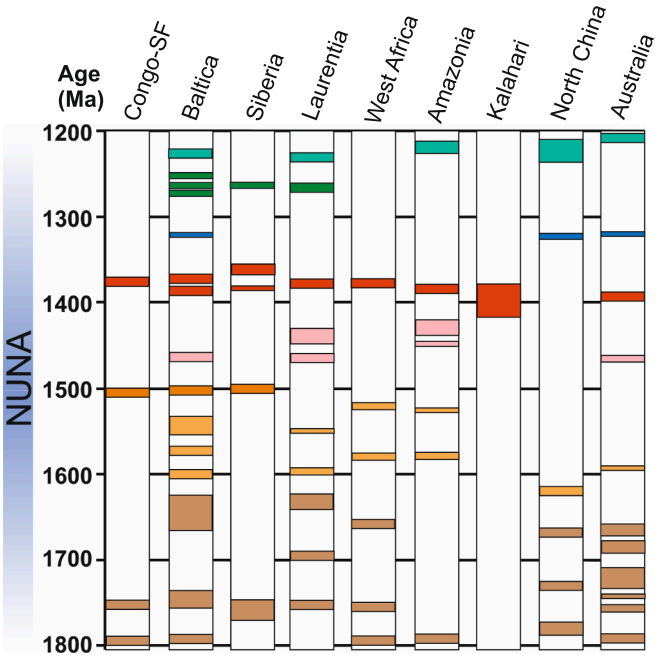

Fig. 10. Large igneous province barcode record for the period of the Nuna cycle (1.8–1.2 Ga) for the selected cratons (data modified from Ernst and Buchan, 2001; de Kock et al., 2019; Teixeira et al., 2019; Ernst et al., 2021; Johansson et al., 2022; Li et al., 2023; Djeutchou et al., 2024).

obtained in São Francisco craton. The ca. 1500 Ma event is represented by the 1507 Ma Curaça mafic dykes and 1501 Ma Chapada Diamantina mafic dykes (Silveira et al., 2013) of the São Francisco craton, and 1502 Ma Humpata sills (Ernst et al., 2013) of the Congo craton. The older events are represented by the 1750 Ma Januária mafic dyke swarm (Chaves and Rezende, 2019) and ca. 1790 Ma Pará de Minas mafic dyke swarm (Cederberg et al., 2016) of the São Francisco craton.

The magmatic barcode of the CSF craton for the Nuna cycle is compared with magmatic barcodes of other major cratons in order to explore for possible "nearest neighbors" (Bleeker, 2003; Bleeker and Ernst, 2006; Ernst and Bleeker, 2010) within the Nuna supercontinent

(Fig. 10). If two blocks share the same age of LIP magmatism then these may have been nearest neighbors; all the while that it is also possible for widely separated blocks to coincidentally share the same age of magmatism (Ernst and Buchan, 2001). However, if multiple LIP ages are shared across cratons then the likelihood of these being nearest neighbors increases (Bleeker and Ernst, 2006). The most convincing match for the CSF craton is with the Siberia and Baltica cratons, which both show ca. 1760–1750 Ma, 1500 Ma and 1380 Ma LIP events, suggesting that these cratons were in proximity during the Nuna cycle. The ca. 1760–1750 Ma event is represented by NW-trending 1770–1750 Ma Timpton dykes (Gladkochub et al., 2022) of the Aldan Shield, inside the Siberian craton, as well as the 1780–1750 Ma Korosten anorthosite and other units (Amelin et al., 1994; Scherbak et al., 1995; Shumlyanskyy et al., 2021) of the Ukrainian Shield, inside Baltica. The 1380 Ma event is represented by the NNW-trending Chieress dyke swarm (Ernst et al., 2000) and Udzha intrusions (Malyshev et al., 2018) in the northern Siberian craton, and 1380–1360 Ma Mashak volcanic rocks (Puchkov et al., 2013) in Baltica. In addition, the ca. 1380 Ma event is globally pronounced and is also observed in West Africa, Laurentia, Australia, and Kalahari. The event is represented in Laurentia by ca. 1380 Ma Zig-Zag Dal basalts and associated intrusions in Greenland (Upton et al., 2005) and by ca. 1380 Ma Salmon River sills and Hart River sills (Abbott, 1997), in West Africa by NE-trending 1400–1360 Ma Tagragra dAkka mafic dykes (Gong et al., 2021), in Kalahari by 1395 Ma Pilanesberg alkaline province (Hanson et al., 2006; Elburg and Cawthorn, 2017), and in West Australia by 1390 Ma Biberkine dolerite dykes of Yilgarn craton (Stark et al., 2018). These ca. 1380 Ma events are suggested to be linked to large-scale continental rifting at ca. 1400–1300 Ma (Zhang et al., 2022), ultimately leading to the break-up of Nuna.

5.2. New Mesoproterozoic pole for Congo-São Francisco craton and its implications for paleogeography of Nuna

5.2.1. The new 1.38 Ga Virei dyke swarm pole for Congo-São Francisco craton

Intriguingly, all dykes with reversed polarity magnetization direction, including the 1385 Ma dated dyke S1633, show tholeiitic composition, and all five dykes with normal polarity magnetization direction share distinctly alkali compositions (Fig. 5), while it is also noted that two alkali dykes (S1836 and S1811) deviate from these groupings. Seven reversed-polarity sites yield a pole at Plat = 23.6°N, Plong = 238.6°E (K = 4.0, A95 = 34.5°), and five normal polarity sites yield a pole at Plat = 57.0°N, Plong = 234.6°E (K = 7.2, A95 = 30.6°) (Fig. 11). Within a given rift setting, magmas with alkali composition are typically considered to be older; but despite the ambiguous reversal test results (test of Heslop and Roberts, 2018), that lends only weak support for the common mean, the overlapping of A95 error ovals of these poles indicate that these directions cannot be distinguished from each other's (Fig. 11). Thus, we combine the virtual geomagnetic poles (VGPs) from these tholeiitic and alkali sub-swarms and calculate a mean pole from all accepted twelve site-mean directions acquired in this study. This yields a 1385 ± 5 Ma pole at Plat = 38.5°N, Plong = 237.3°E (K = 4.5, A95 = 23.2°). The VGPs are scattered (Fig. 11), which lowers the statistical quality of the mean pole (see section 5.2.2.).

Based on rock magnetic analyses and behavior of samples during the demagnetization, the characteristic remanent magnetization is interpreted to be carried by magnetite. Although the 1385 Ma Virei pole is lacking a positive baked contact test in the strict sense, the other dyke swarms in the same region, such as 1100 Ma Huila-Epembe dyke swarm (Fig. 3), have magnetizations that are systematically different according to their younger age (Salminen et al., 2018) (Fig. 11); and therefore, the reliability of the new 1385 ± 5 Ma pole from the Virei dykes is supported by a regional age-consistency test (Buchan, 2014). Moreover, the adjacent Kaoko belt (Fig. 3), which was orogenically active during the Ediacaran–Cambrian time, is a likely source of remagnetization in the subsequent geological history of the region, and we observe its effects in four of our westernmost sites. Yet, the modal Virei swarm magnetization is distinct from WSW or NW downward magnetic remanence directions interpreted as Ediacaran–Cambrian overprint directions by comparison to the Congo craton's apparent polar wander path from that time interval (Trindade et al., 2021) (Fig. 11). Comparison to Gondwanan poles (in African coordinates, Torsvik et al., 2012) shows that the inverted polarity Virei poles are close to Permian Gondwanan poles (Fig. 11), but we interpret this as coincidence as there is no evidence of Permian tectonism in the study area (e.g., de Wit et al., 2018; Macgregor, 2018; Lovecchio et al., 2020). Permian rifting in the Congo craton is limited to

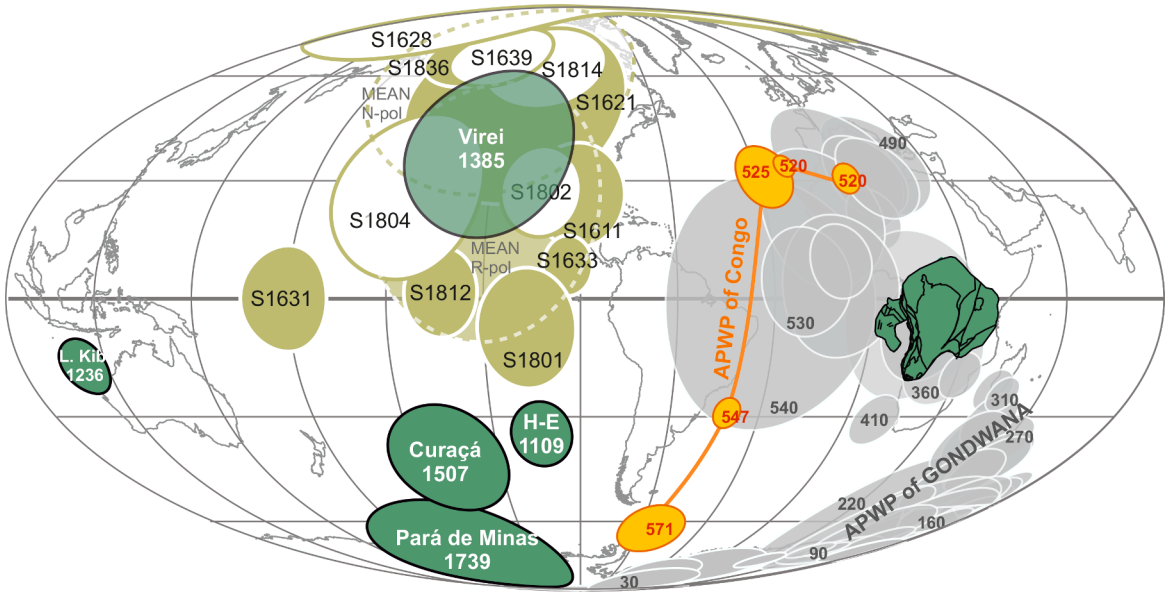

Fig. 11. The site mean virtual geomagnetic poles (VGPs) for the dykes of the 1385 Ma Virei swarm (pale green, Table 3) together with the high-quality Proterozoic paleomagnetic poles of CSF craton (dark green, Table 4), with ages in Ma. Also shown Cambrian paleomagnetic poles of CSF craton (yellow, Trindade et al., 2021), and Gondwana APWP in African co-ordinates (grey, Torsvik et al., 2012). For the VGPs of the Virei swarm: closed and open pole symbols indicate the site-number-labeled ChRM directions of NW-up and SE-down (inverted), respectively. Poles with dashed lines are mean R- and N-polarity poles. S1633 represents the geochronology site. (For interpretation of the references to color in this figure legend, the reader is referred to the web version of this article.)

Table 4
Selected global paleomagnetic poles from the CSF and/or the Nuna interval.

Rock unit/Pole name	Code	Age (Ma)	Plat (°)	PLong (°)	A95 (°)	R-score	Pole reference
Amazonia							
Colider Volcanics	Colider	1789 ± 7	−63.3	298.8	11.4	(1010110)4	Bispo-Santos et al., 2008
Avanavero (mafic rocks)	Avana	1788.5 ± 2.5	48.4	208.9	9.2	(1111101)6	Bispo-Santos et al., 2014
Mucajaí Complex	Mucajaí	1538 ± 5; 1535 ± 7.5; 1527 ± 7; 1526 ± 2;1527 ± 2	38.2	180.1	12.6	(1110101)5	Bispo-Santos et al., 2020
Rio Branco (sedimentary rocks)	R Bran	1544–1440	45.5	90	6.5	(0011111)5	D'Agrella-Filho et al., 2016
Salto do Céu Intrusions	S Céu	1439 ± 4	56	98.5	7.9	(1111110)6	D'Agrella-Filho et al., 2016
Nova Guarita Dykes	N Gua	1419 + 3/-4	47.9	65.9	6.6	(1111110)6	Bispo-Santos et al., 2012
Indiavai Gabbro	Indi	1416 ± 7	57	69.7	8.9	(1110000)3	D'Agrella-Filho et al., 2012
Baltica							
Hoting Gabbro	Hot	1786 ± 10	43.0	233.3	10.9	(1111101)6	Elming et al., 2009
Shoksha Sandstones	Shok	1770 ± 12	39.7	221.1	4.0	(1111111)7	Pisarevsky and Sokolov, 2001
Ragunda Dykes (Group 1) + Strömsbro Rapakivi + Strömsbro Dykes + Rödö Rapakivi	Rag1	1497 ± 6; 1500 ± 19; 1505 ± 12; 1514 ± 5	12.7	190.1	10.2	(1111101)6	Salminen et al., 2021
Mashak Suite	Mashak	1366 ± 6; 1384 ± 3; 1386 ± 5; 1386 ± 6	1.8	193.0	14.8	(1001110)4	Lubnina, 2009
Bornholm Group I Dykes	Bornh	1326 ± 10	5.0	166.0	6.6	(1111111)7	Luoto et al., 2021
Congo - São Francisco							
Pará de Minas Dykes (rot to Congo)	P de Min	1798 ± 4; 1793 ± 18; 1791 ± 7	−70.6	202.8	17.0	(1011100)4	D'Agrella-Filho et al., 2020
Curaça Dykes and baked rocks (rot to Congo,)	Curaça	1506.7 ± 6.9	−41.6	221.4	15.8	(1111110)6	Salminen et al., 2016a
Virei Dykes	Virei	1385 ± 5	38.5	237.3	23.2	(1010110)4	This work
Kunene Complex		1371 ± 2.5; 1376 ± 2	−03.0	255.0	17.0	(1000011)3	Piper, 1974
Late Kibaran Intrusions		1236 ± 24	−17.0	112.7	7.0	(0010001)2	Meert et al., 1994
Huila-Epembe Dykes		1104; 1110 ± 3;1109 ± 3	−34.7	256.5	8.7	(1111101)6	Salminen et al., 2018
Laurentia							
Dubawnt Group	Dub	1820–1750	7.0	277.0	8.0	(0111110)5	Park et al., 1973
Cleaver Dykes	Clea	1745–1736	19.4	276.7	6.1	(1111101)6	Irving, 2004
Western Channel Diabase	W Chan	1592 ± 31;1590 ± 4	9.0	245.0	8.6	(1011101)5	Irving et al., 1972;Hamilton and Buchan, 2010
St.Francois Mountains	St Fran	1476 ± 16	−13.2	219.0	8.0	(0111101)5	Meert and Stuckey, 2002
Michikamau Intrusion	Mic Intr	1460 ± 5; 1400 ± 50; 1479 ± 101	−1.5	217.5	6.6	(1011111) 6	Emslie et al., 1976
Spokane Formation	Spok Fm	1457.5 ± 12.5;1468 ± 2	−24.8	215.5	4.7	(1111101) 6	Elston et al., 2002
McNamara Formation	McNam	1401 ± 6	−13.5	208.3	6.7	(1111111)7	Elston et al., 2002
Pilcher Formations	Pil	1365 ± 3;1401 ± 6	−19.2	215.3	7.7	(0111101)5	Elston et al., 2002
Victoria Fjord Dolerite Dykes (rot to Laur.)	Vict Fjo	1382 ± 2	14.2	219.9	5.9	(1011111)6	Abrahamsen and Van der Voo, 1987
Midsommersö Dolerite (rot to Laur.)	Mids	1382 ± 2	9.3	229.9	5.1	(1011111)6	Marcussen and Abrahamsen, 1983
Zig-Zag Dal Basalts (rot to Laur.)	Zig Zag	1382 ± 2	14.2	231.2	3.8	(1011111)6	Marcussen and Abrahamsen, 1983
Siberia							
Kuonamka Dykes	Kuonam	1503 ± 5	−6	54	19.8	(1000101)3	Ernst et al., 2000
West Anabar Intrusions	W Anab	1502 ± 2;1503 ± 2	−25.3	61.4	4.6	(1010101)4	Evans et al., 2016
North Anabar Intrusions	N Anab	1483 ± 17	−23.9	75.3	7.5	(0011101)4	Evans et al., 2016
Sololi-Kyutingde Intrusions	Kyo Sol	1473 ± 24	−33.6	73.1	10.4	(0011101)4	Wingate et al., 2009
Chieress Dyke (virtual geomagnetic pole)	Chier	1384 ± 2	4	258	6.7	(1010101)4	Ernst et al., 2000
North Australia							
Hart Dolerite	Hart	1797 ± 11;1792	−5.3	181	12.0	(1111111)7	Kirscher et al., 2019
Elgee-Pentecost Formation (combined)	Elg	1790–1730	−5.4	211.8	3.2	(0111100)4	Schmidt and Williams, 2008
Peters Creek Volcanics (upper part)	Pet	1729–1725	−26.0	221.0	4.8	(1111111)7	Idnurm, 2000
Wollogorang Formation	Wol	1730–1723	−17.9	218.2	7.2	(1011110)5	Idnurm et al., 1995
Balbirini Dolomite (upper part)	Balb	1589 ± 3	−52.0	176.1	7.5	(1000101)3	Idnurm, 2000
Mt. Isa Metamorphosed Dykes	Mt. Isa	1550–1500	−79.0	110.6	8.4	(0100010)2	Tanaka and Idnurm, 1994
Derim Derim Sills	Derim	1312.9 ± 0.7;1327.5 ± 0.7	−76.5	120.2	15.0	(1111101)6	Kirscher et al., 2020
North China							
Xiong'er Group	Xio	1780 ± 10	50.0	272.7	4.9	(1011111)6	Zhang et al., 2012
Taihang Dykes (Central zone)	Tai	1769 ± 2.5	47.9	275.2	4.0	(1011111)6	Halls et al., 2000
Yinshan Dykes	Yin	1769 ± 2.5	32.3	248.3	2.0	(1111101)6	Halls et al., 2000; Xu et al., 2014
Yangzhuang Formation	Yang1	1560–1437	17.3	214.5	5.7	(0011111)5	Wu et al., 2005
Yangzhuang Formation	Yang2	1560–1437	2.4	190.4	11.9	(0011111)5	Pei et al., 2006
Tieling Formation	Tie	1437 ± 21	11.6	187.1	6.3	(0111101)5	Wu et al. 2005
Yanliao Mafic Sills	Yanl	1323; 1320 ± 4; 1324 ± 5;1325 ± 5	−5.9	179.6	3.6	(1011101)5	Chen et al., 2013
West Africa							
Iguerda NW-SE Dyke (virtual geomagnetic pole)	Igu	1747 ± 4	4	82.1	2.5	(1010101)4	Neres et al., 2016
Tagragra d'Akka NE-SW Dykes	Tagragra	1400–1360	−87.4	224.7	7.9	(0111101)5	Gong et al., 2021

Code = Code in Figs. 12 and 13, Plat = paleomagnetic pole latitude, Plon = paleomagnetic pole longitude, A95 = radius of 95 % confidence cone of paleomagnetic pole, R-score = reliability criteria of paleomagnetic poles following Meert et al. (2020).

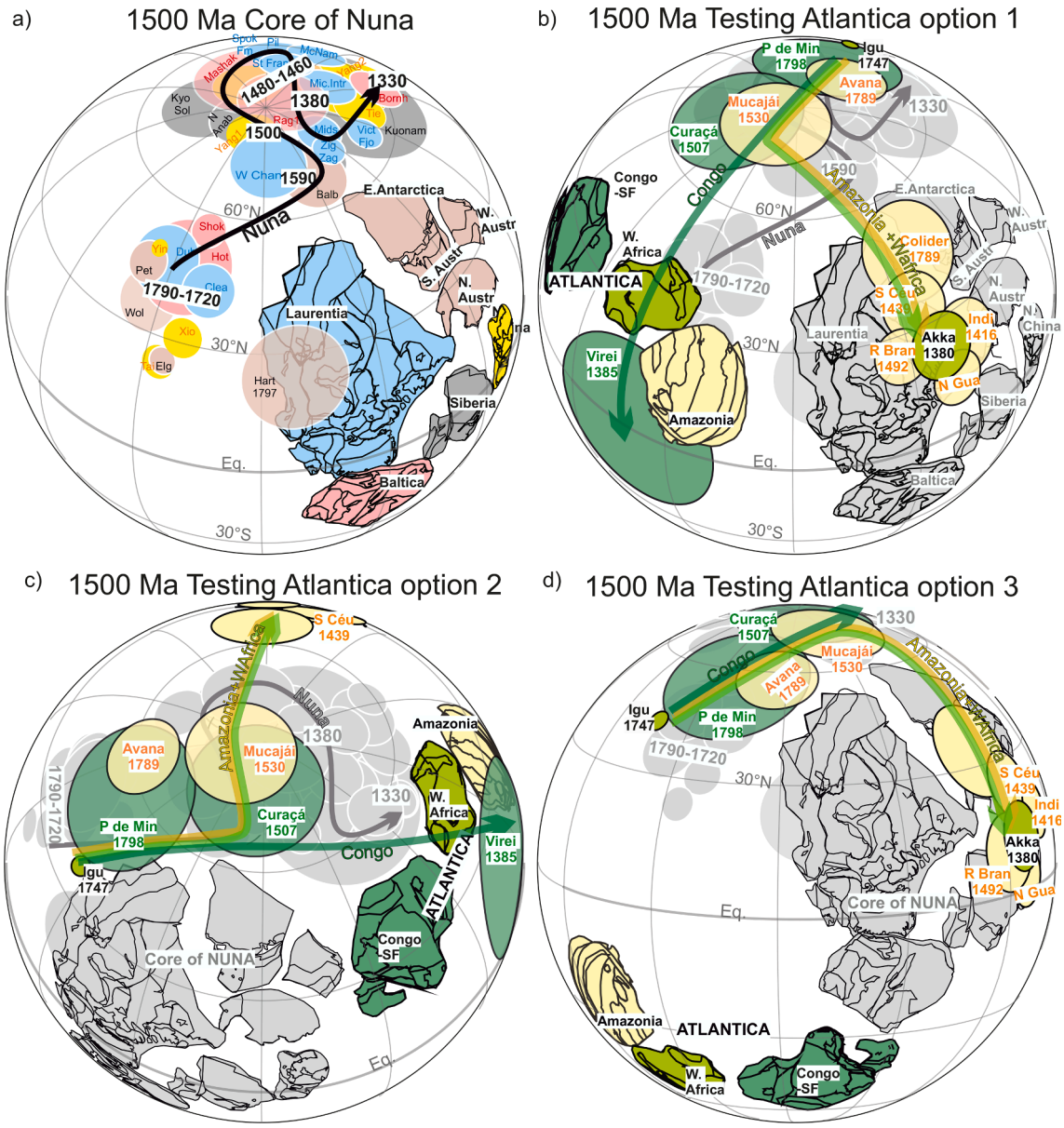

Fig. 12. Testing an Atlantica-like configuration, and its relation to Nuna. (a) Reconstruction of the core of Nuna at 1500 Ma with Laurentia, Baltica, Siberia, North China and proto-Australian cratons. Poles' A95 regions are color coded with the cratons. Black arrow indicates a common apparent polar wander path for Nuna cratons with black numbers showing the age of the poles in Myr. (b) Reconstruction of Atlantica option 1 after Elming et al. (2021) (polarity of the Atlantica poles inverted from Table 4), (c) Reconstruction of Atlantica option 2 (polarity of the Atlantica poles inverted from Table 4), (d) Reconstruction of Atlantica option 3 (polarity of the Atlantica poles as in Table 4). In each of the Atlantica options 1–3, the discordance of the Virei pole with coeval poles from other Atlantica blocks (e.g., Tagragra dAkka from West African craton) implies that if such an Atlantica reconstruction existed at ca. 1500 Ma, then it could not have persisted until ca. 1380 Ma (see discussion of these options in 5.2.3.1). The comparison of Atlantica and Nuna poles also show that the all the Atlantica options require substantial change in relative location of the Atlantica landmass and Nuna between 1500 and 1385 Ma. Atlantica poles' A95 regions are color coded with the cratons: Amazonia – pale yellow; CSF – dark green, West Africa – light green with ages in Myr. Nuna cratons and poles are indicated with grey. Used poles are listed in Table 4. Euler rotation parameters (Elat°/Elon°/Erot°) between the cratons: Amazonia to Laurentia in Atlantica option 1 (-7.0/126.9/125.9), Amazonia to Laurentia in Atlantica option 2 (-50.1/-98.3/143.9), Amazonia to Laurentia in Atlantica option 3 (-57.4/141.1/301.4), West Africa to Amazonia (Table 5, all the Atlantica options), Congo-São Francisco (SF) to Amazonia (-12.3/-172.2/148.9) (all the Atlantica options), other cratons as in Fig. 13 (Table 5). (For interpretation of the references to color in this figure legend, the reader is referred to the web version of this article.)

southern and eastern parts of the craton and there is no associated magmatism. Moreover, Permian overprints are not observed in the 1.1 Ga Huila dykes sampled in the same region as the Virei dykes (Fig. 3) (Salminen et al., 2018). The magnetic reversals do not pass the test of McFadden and McElhinny (1990) and yield ambiguous results from the test of Heslop and Roberts (2018). Strictly, the new Virei pole scores only four of the seven updated Van der Voo (1990) reliability criteria (R1234567: 1010110) (Table 4) (Meert et al., 2020). However, robustness of pole is supported by a well-defined age, a regional age-consistency test, presence of reversals, usage of modern analysis techniques; and while the inverted pole is overlapping with the Gondwanan Permian poles, there is no indication of Permian rifting and magmatism in the sampling area. Therefore, we suggest that our Virei pole serves utility towards the placement of Congo-São Francisco craton within Nuna and through its early stages of breakup.

5.2.2. *Scatter of the Virei virtual geomagnetic poles*

The scatter of the Virei swarm VGPs could in principle arise from

several causes, such as (1) unremoved secondary component (Palmer, 1970), (2) inadequate sampling of paleosecular variation (Buchan and Halls, 1990), (3) unusual behavior of the geomagnetic field (e.g., Palmer, 1970; Pesonen and Nevanlinna, 1981; Abrajevitch and Van der Voo, 2010), (4) true polar wander (e.g., Evans, 2003) or (5) a slight age difference, less than the error rage of U-Pb age, between the dyke sites combined with rapid plate motion (e.g., Swanson-Hysell et al., 2014). In the case of our modal Virei direction, unremoved secondary components are conceivable but unlikely to be the explanation for the scatter, because the ChRM component forms straight lines to the origin (Fig. 8) and no other remanence-carrying minerals than magnetite are observed in the samples (Fig. 7). Inadequate sampling of paleosecular variation is also unlikely because both normal and reversed polarity directions were obtained from the Virei dykes, and both polarities show similar scatter in

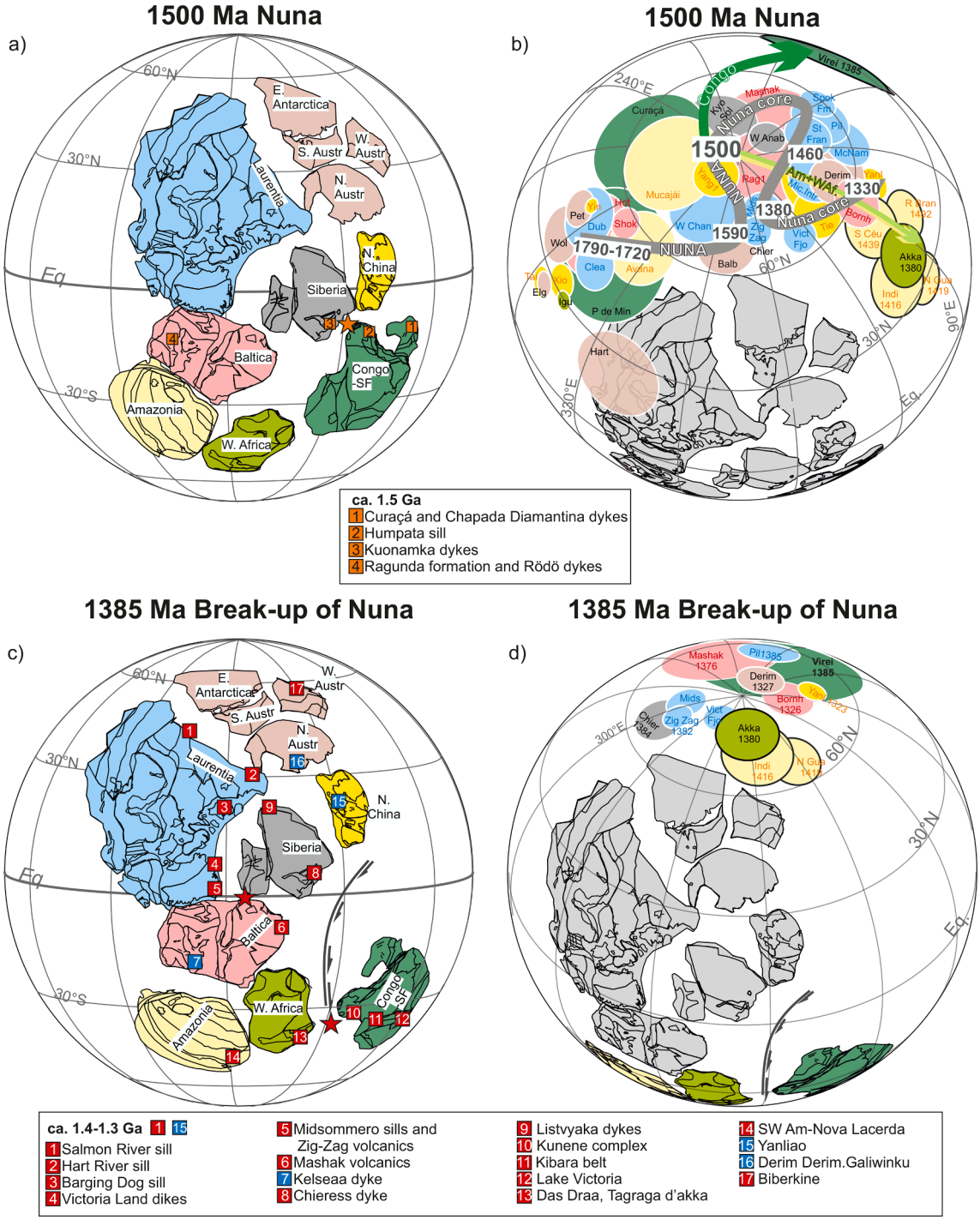

Fig. 13. (a) Paleogeographic reconstruction of Nuna at 1500 Ma with global large igneous province records and (b) with paleomagnetic poles (Table 4). Color of the paleomagnetic poles match those of cratons in (a). Arrows indicate apparent polar wander paths: Nuna – grey, CSF – dark green, Amazonia – pale yellow, West Africa – light green. (c) Paleogeographic reconstruction of break-up of Nuna at ca. 1380 Ma with global large igneous province records and (d) with paleomagnetic poles (Table 4). Color of the paleomagnetic poles match those of cratons in (c). Used Euler parameters are listed in Table 5. Number are ages in Myr. SF – São Francisco. Stars indicate possible plume centre for large igneous provinces. (For interpretation of the references to color in this figure legend, the reader is referred to the web version of this article.)

directions. Unusual behavior of the geomagnetic field, for example a permanent non-dipolar field contamination (e.g., Pesonen and Nevanlinna, 1981; Veikkolainen et al., 2014) or switching of the geomagnetic field between dominant axial dipole field and an equatorial dipole field (i.e. as Ediacaran, Abrajevitch and Van der Voo, 2010) may cause scatter in the data, but such a process might be expected to cause pronounced asymmetry between normal and reversed polarity sites. Using paleomagnetic remanent magnetization of the 2470–2455 Ma Matachewan dykes, the 1270 Ma Mackenzie dykes and the 720 Ma Franklin dykes, Panzik and Evans (2014) produced statistical geomagnetic field models and showed that the geocentric axial dipole hypothesis is viable during the Proterozoic, including during the Nuna cycle, and those data do not support significant and stable global non-dipole field components. Recently, Veikkolainen and Pesonen (2021) suggested that during the Nuna cycle the geomagnetic field could have had octupole components as large as 23 %, but their results can also be explained with Nuna cratons occupying near-equatorial latitudes during part of this time. The coeval 1382 ± 2 Ma (Upton et al., 2005) paleomagnetic data from Greenlandic Midsommersø dolerites (Marcussen and Abrahamsen, 1983), Zig-Zag Dal basalts (Marcussen and Abrahamsen, 1983), and Victoria Fjord dolerites (Abrahamsen and Van Der Voo, 1987) do not show as much scatter as the Virei swarm, and for this reason it is unlikely that the scatter of the Virei dyke swarm VGPs is caused by a global phenomenon. The same reasoning would apply to a true polar wander event, which should be recognized globally; and such an event is therefore unlikely to be the explanation for the scattered Virei data.

A large scatter of the VGPs was also previously obtained from twelve different sites within the dark anorthosite of the 1385–1375 Ma Kunene Complex sampled in Angola (Piper, 1974). Piper (1974) suggested that this scatter was because of continental drift during the cooling of the Complex. However, this was later ruled out by Larson (2015), who noted that Piper (1974) used outdated methods and did not correct sites to paleohorizontal inside the Kunene Complex. Piper (1974) collected five block samples per site and prepared one to three paleomagnetic cores (specimens) from each sample. He used an alternating field demagnetization technique in 10 mT field steps until 160 mT for two specimens per site, and accordingly chose the level for blanket field demagnetization for the rest of the specimens from each site. Moreover, none of the directions from the Kunene Complex were analyzed with a modern vector subtraction technique (Piper, 1974). It is nevertheless intriguing that despite modern paleomagnetic analysis used in the present study, our results reproduce the scatter obtained by Piper (1974) from the coeval Kunene Complex. As it is unlikely that a global phenomenon (i.e., non-dipolar or unstable geomagnetic field or true polar wander) caused the scatter of the VGPs of the Virei swarm, we suggest that a slight age range among the dykes combined with non-negligible plate motion could be a plausible explanation.

5.2.3. *Implications for paleogeography of Nuna*

As discussed in section 5.2.1, the reliability of the new 1385 Ma Virei pole is supported by a well-defined age, a consistency test (Buchan, 2014), and the use of modern demagnetization analysis techniques. Our paleomagnetic result therefore adds to the small number of Mesoproterozoic poles of CSF craton reviewed in Salminen et al., (2016a) and Trindade et al. (2021). For the CSF craton there are now three robust poles, including the Virei pole, through the Nuna cycle (Fig. 11). By including our new pole with quality-filtered poles from the other cratons during the Nuna interval (Table 4) we can model the kinematics of CSF craton in the Nuna cycle and test previous proposed configurations.

5.2.3.1. Testing the Atlantica landmass during the Nuna cycle. A postulated ancestral "Atlantica" landmass, with southern Atlantic-bordering cratons in an original configuration similar to that of Gondwana (Rogers, 1996), has already been challenged by Paleoproterozoic paleomagnetic data obtained mainly from Amazonia (+West Africa) and Río de la Plata cratons (D'Agrella-Filho et al., 2011; Rapalini et al., 2015). However, Paleoproterozoic (2080–2000 Ma) paleomagnetic data from the alleged Atlantica cratons permits the existence of the landmass including CSF, Amazonia-West Africa and Río de la Plata cratons, in a modified relative configuration compared to their relative Gondwana fit (Rapalini et al., 2015; Franceschinis et al., 2019; Rapalini et al., 2021). Recently, also using high-quality global paleomagnetic data, Elming et al. (2021) suggested that an Atlantica-like landmass, separate from other Nuna cratons, was possible at 1490–1260 Ma during the Nuna cycle. The study of Elming et al. (2021) was based only on poles from one of the Atlantica cratons for each considered timeslot: at 1490 Ma, 1350 Ma, and 1260 Ma. For their 1490 Ma reconstruction, a high-quality 1507 Ma pole from the Curaça dykes (Salminen et al., 2016a) of the CSF

Table 5
Euler rotation parameters (Elat, Elong, Erot) used in the reconstructions.

Craton	Time (Ma)	Elat (°)	Elong (°)	Erot (°)	In relative to	Reference
Laurentia	1385	14.34	−067.11	−87.48	Rotation axis	This work
Laurentia	1500	18.93	−055.36	−101.69	Rotation axis	This work
Amazonia	1385	−52.04	108.14	−104.35	Laurentia	This work
Amazonia	1500	−53.38	087.19	−97.68	Laurentia	This work
Baltica	1385	47.50	001.50	49.00	Laurentia	Evans and Pisarevsky, 2008
Baltica	1500	47.50	001.50	49.00	Laurentia	Evans and Pisarevsky, 2008
Congo	1385	−02.56	064.08	−116.11	Laurentia	This work
Congo	1500	23.49	059.73	−154.28	Laurentia	Modified from Salminen et al 2016a
Siberia	1385	75.04	117.32	160.17	Laurentia	This work
Siberia	1500	75.04	117.32	160.17	Laurentia	This work
North China	1385	36.90	014.60	38.20	Laurentia	Kirscher et al. (2020)
North China	1500	36.90	014.60	38.20	Laurentia	Kirscher et al. (2020)
West Africa	1385	02.67	−020.55	−209.53	Amazonia	This work
West Africa	1500	02.24	−019.96	−214.85	Amazonia	This work
North Australia	1385	38.00	090.00	103.00	Laurentia	Kirscher et al., 2019
North Australia	1500	38.00	090.00	103.00	Laurentia	Kirscher et al., 2019
West Australia	1385	−20.00	135.00	40.00	North Australia	Li and Evans, 2011
West Australia	1500	−20.00	135.00	40.00	North Australia	Li and Evans, 2011
South Australia	1385	−20.00	135.00	40.00	North Australia	Modified from Evans and Mitchell, 2011, Pehrsson et al., 2016
South Australia	1500	−20.00	135.00	40.00	North Australia	Modified from Evans and Mitchell, 2011, Pehrsson et al., 2016
Other rotations within the blocks						
Aldan		60.00	115.00	25.00	Anabar before Devonian	Evans, 2009
Greenland		67.50	241.50	−13.80	Laurentia	Roest and Srivastava, 1989
Mawson block, E Antarctica		01.30	037.70	30.30	South Australia	Collins and Pisarevsky, 2005
São Francisco		46.80	329.40	55.90	Congo	McElhinny et al., 2003

craton was used. For their nominal 1350 Ma reconstruction, the high-quality, but 60 Ma older, pole of 1416 Ma Indiavai gabbro (D'Agrella-Filho et al., 2012) from Amazonia craton was used. This reconstruction is supported with the coeval, but lower quality 1419 Ma Nova Guarita intrusives pole (Bispo-Santos et al., 2012) of Amazonia. For the 1270 Ma reconstruction in Elming et al. (2021), a low-quality pole from the Late Kibaran intrusions (Meert et al., 1994) from the CSF craton was used. Coeval pole pairs provide more robust tools for testing the lifecycle of relative cratonic configurations, than single poles of only approximately similar ages from different cratons. With the new Virei pole from this study, there are now two pole pairs, ca. 1530–1500 Ma and 1385–1380 Ma, for CSF and Amazonia + West Africa cartons (Table 4).

We first test a configuration whereby the Atlantica-like landmass is separate from other Nuna cratons as in Elming et al. (2021) (Fig. 12b) and use the typical relative configuration of Congo and São Francisco (McElhinny et al., 2003), but where the relative configuration of Amazonia and West Africa follows the recent suggestion of Gong et al. (2021). In this new Amazonia-West Africa configuration the northeast West African craton is reconstructed against southwest Amazonian craton. To test this Atlantica proposition (Atlantica option 1), the poles of the Congo-São Francisco and Amazonia-West Africa are inverted (Table 4). For the pole comparison at ca. 1500 Ma (Fig. 12b), the 1530 Ma Mucajaí pole places Amazonia-West Africa craton at low to equatorial latitudes, and similarly the 1507 Ma Curaça pole places Congo-São Francisco craton at low to equatorial northern latitudes, oriented such that the eastern (Tanzania) sector of Congo craton is adjacent to the southern part of the West Africa craton (Fig. 12b). In addition to the ca. 1500 Ma pole pair, the ca. 1800–1750 Ma poles (1789 Ma Avanavero pole of Amazonia craton, 1747 Ma Iguerda NW-SE dyke pole of West Africa, and 1798 Ma Pará de Minas pole of São Francisco craton; inverted poles from the Table 4) are overlapping in this configuration, but the ca. 1420–1380 Ma poles: 1419 Nova Guarita and 1416 Indiavai poles of Amazonia craton and 1380 Ma Tagragra d'Akka pole of West Africa craton are far apart from the 1385 Ma Virei pole of Congo craton (Fig. 12b). This indicates that while the Atlantica landmass is paleomagnetically plausible at 1798–1500 Ma, the paleomagnetic data would indicate separation of Congo-São Francisco craton from Amazonia (+West Africa) before 1380 Ma. The comparison of Atlantica and Nuna poles also show that the tested 1500 Ma reconstruction (Atlantica option 1) (Fig. 12b) requires substantial change in relative location of the Atlantica landmass and Nuna at 1790–1385 Ma. In Atlantica option 2 we rotate Atlantica poles (inverted poles from Table 4, as in Atlantica option 1) so that ca. 1800–1750 Ma poles and 1500 Ma poles of Atlantica are overlapping with the coeval poles of the Nuna core (Atlantica option 2, Fig. 12c). This results in a configuration where Atlantica cratons are reconstructed onto intermediate northern latitudes so that northern CSF is facing South Australian craton. The comparison of Atlantica and Nuna poles also show that the tested 1500 Ma reconstruction (Atlantica option 2) (Fig. 12c) requires substantial change in relative location of the Atlantica landmass and Nuna at 1500–1385 Ma. In the third option we use a different polarity option for the Atlantica poles compared to the Atlantica options 1 and 2, rotating the poles of Atlantica cratons so that ca. 1800–1750 Ma poles and 1500 Ma poles of Atlantica again overlap with coeval poles of the Nuna core (Fig. 12d). This results in a configuration (Atlantica option 3) where Atlantica cratons are reconstructed onto intermediate southern latitudes so that the western part of the São Francisco craton faces south Baltica. Also in Atlantica option 3, paleomagnetic poles require substantial change in the relative location of the Atlantica landmass and Nuna at 1500–1385 Ma. Although, separate plate motions are always conceivable in a myriad of combinations when interpreting paleomagnetic poles, a more tractable hypothesis to test is one of long-lived tectonic association. Inspired by the matches of magmatic barcodes (see section 5.1.), which at 1500 Ma show the most convincing matches among Congo-São Francisco craton, Siberia and Baltica, we follow Rapalini et al. (2015) by suggesting that Atlantica cratons were in proximity to other Nuna cratons during the Nuna cycle. In the next section we propose reconstructions of the Congo-São Francisco craton onto the paleo-southeast side of the Nuna supercontinental landmass.

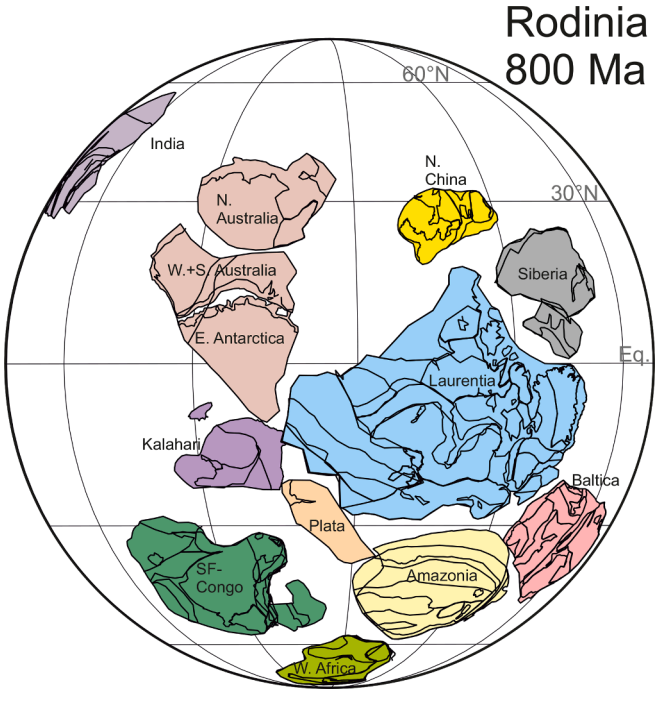

Fig. 14. Rodinia supercontinent at 800 Ma (modified from Mitchell et al., 2021).

5.2.3.2. Paleogeography of Nuna and its implications. Our refined Nuna model, based on high-quality ca. 1790–1500 Ma paleomagnetic data (Table 4), is shown in Fig. 13 a-b. There is a common consensus that Baltica and Laurentia formed the core of Nuna together with the Siberian craton. An increased line of evidence, both geologically (Gower et al., 1990) and paleomagnetically (Buchan et al., 2000; Salminen and Pesonen, 2007; Evans and Pisarevsky, 2008; Salminen et al., 2009; Evans and Mitchell, 2011; Pisarevsky and Bylund, 2011; Salminen et al., 2014; Salminen et al., 2016b), support a North Europe North America (NENA) connection at least from 1.75 to 1.27 Ga. Siberia is commonly shown either in a tight fit with northern Laurentia (Wu et al., 2005; Evans and Mitchell, 2011; Ernst et al., 2016) or with ca. 1500 km separation (Pisarevsky et al., 2008; Pesonen et al., 2012). We are reconstructing Siberia tightly to the Laurentian craton using slightly modified rotation parameters from (Evans et al., 2016) (Fig. 13ac, Table 5). Proto-Australian cratons are shown in their commonly accepted proto-SWEAT connection close to the southwestern margin of Laurentia (Pisarevsky et al., 2014; Kirscher et al., 2020). The North China craton is reconstructed in a tight fit with proto-Australian cratons following Kirscher et al. (2020), and in our chosen Laurentia-Siberia reconstruction the North China craton is also tightly juxtaposed with the Anabar-Angara part of the Siberian craton. In our 1500 Ma Nuna model we maintain the relative configuration between the CSF craton and Amazonia-West Africa craton, as in our Atlantica landmass test above. In accordance with barcode matching of Siberia and Congo-São Francisco at 1500 Ma, we juxtapose the southwest Congo craton with the northwester part of the Anabar-Angara part of the Siberia craton, so that 1500 Ma large igneous provinces (LIPs) of both Congo and Siberian cratons were emplaced in proximity with each other at that time and essentially in the relative configuration proposed by Ernst et al. (2013b) (Fig. 13a, Table 5). In our model, the Amazonian craton is reconstructed close to the southwestern margin of Baltica, which is also geologically

permissible based on the proposed similar geological accretion history of these cratons within the Nuna cycle (Johansson, 2009). The 1790–1720 Ma paleomagnetic poles from CSF, Amazonia-West Africa, Baltica, Laurentia, proto-Australia and North China cratons are overlapping (Fig. 13b) and therefore support their cratonic connections for at least 200 million years (until ~ 1500 Ma); while highly dispersed ca. 1420–1380 Ma poles imply subsequent breakup and substantial drift of CSF and Amazonia + West Africa cratons from the Nuna between ca. 1500 and 1380 Ma (Fig. 13b). Nonetheless, since proximity of all these cratons is suggested by numerous LIP barcode matches during this younger time period, we propose a distinct arrangement of marginal Nuna blocks at the time of the 1380-Ma LIP emplacement (Fig. 13c). The locations of ca. 1385 Ma LIPs in our refined Nuna reconstruction are broadly similar to that proposed by Zhang et al. (2022) but now with a modified and more precisely paleomagnetically constrained azimuthal orientation of the CSF craton that requires two separate plumes: one at the northeastern margin of Baltica and the other at the southern margin of CSF craton (Fig. 13c). These would be temporally related to the early stages of the Nuna break-up (Kirscher et al., 2020; Gong et al., 2021), which in our model occurred after a precursor tectonic modification of the supercontinent's margin. A more recent analog, though by comparison smaller in magnitude, is provided by the multi-stage opening of the modern Indian Ocean, which began with highly oblique dextral rifting between an eastern Gondwanaland (Madagascar + India + Antarctica + Australia) and western Gondwanaland (Africa + South America) (Thompson et al., 2019), coincident with arrival of the mid-Jurassic Karoo LIP; and those blocks maintaining their proximity prior to a large-scale fragmentation that was coincident with emplacement of the early Cretaceous Comei-Kerguelen-Bunbury LIP. .

The suggestion of an extensional origin for the Kunene Complex (e.g., Mayer et al., 2004; Drüppel et al., 2007; McCourt et al., 2013; Kröner and Rojas-Agramonte, 2017; Jelsma and McCourt, 2018) and for a short-lived Kibaran event (Tack et al., 2010) supports a 1385–1375 Ma break-away of the CFS craton from Nuna. However, emplacement of Kunene Complex and Kibaran events in an arc setting is alternatively considered by others (e.g., Kokonyangi et al., 2006; Lehmann et al., 2020). According to the southern Indian Ocean break-up analogy described above, occurring inland of a proto-Pacific subduction zone, there need not be mutual exclusion of mantle plumes and suprasubduction settings along the margins of fragmenting supercontinents. Furthermore, the 'asthenospheric' and alkali geochemical signatures of Virei dykes with normal polarity magnetization direction are more consistent with a continental rift setting. Such rift-magmatism could precede increased degrees of shallower decompression mantle melting during a final break-up stage, generating more tholeiitic magmas for consistently reversed polarity Virei dykes, with slightly more 'lithospheric' signatures from the incorporation of either continental crusts or sub-continental lithospheric mantle. This sequencing is consistent with the dated reversed polarity dyke also being tholeiitic, and thereby more likely break-up related, while alkali dykes may have been generated by earlier rift magmatism during the emplacement of a 1384–1375 Ma Kunene LIP (Bybee et al., 2019). While incompatible element patterns of the dykes (Fig. 6a) argue all dykes being part of the same swarm and comparison to modern rift systems, such as East African rift system, indicate that both alkaline and tholeiitic magmas can be produced within the given age range for the Virei swarm, further geochronology of the normal-polarity Virei dykes may determine whether these more alkali dykes are indeed part of the same swarm.

In the context of our kinematic model, the 1385 Ma Virei pole requires a substantial transform motion and large-magnitude azimuthal rotation (~85°) of CSF between 1500 Ma and 1385 Ma. It also indicates a large displacement and rotation of CSF relative to Laurentia on the way to its configuration in Rodinia (Fig. 13c and 14). Amazonia, another purported "Atlantica" craton, has also been suggested to rotate ca. 180° relative to Laurentia prior to its Rodinia assembly (D'Agrella-Filho et al., 2016). Moreover, Gong et al. (2021) proposed a similar ca. 180° relative rotation between West Africa and Amazonia cratons over supercontinent cycles. Gong et al. (2021) pointed out that this kind of large-scale azimuthal rotation is not a typical feature of large continental blocks, and during the past few hundred million years large cratons have experienced smaller amounts of relative azimuthal rotation. We stress that such large-scale relative rotations are to be expected when orthogonal rifting/convergence is interspersed with transform motions through time intervals spanning hundreds of millions of years (e.g., Müller et al., 2016; Gong et al., 2021).

6. Conclusions

A large WNW-trending mafic dyke swarm, related to the Kunene Complex, has been identified near the town of Virei in southwest Angola. The Virei swarm yields a magmatic U-Pb baddeleyite age of 1385 ± 5 Ma and is considered to belong to the Kunene-Kibaran large igneous province (LIP) of the Congo craton. This result adds to the globally pronounced ca. 1380 Ma LIP events that are also identified in Siberia, West Africa, Baltica, Laurentia, Amazonia, and Kalahari. A new, reliable paleomagnetic pole for Congo-São Francisco craton was obtained from the Virei dyke swarm that may be composed of a rift-related normal polarity sub-swarm with more alkali composition and a reversed polarity sub-swarm that was tholeiitic and more breakup-related. Their overall mean pole constrains the Congo-São Francisco craton at low- to mid-latitudes during the time of magnetization.

Comparison of global 1790–1385 Ma robust paleomagnetic poles supports the proximity of Congo-São Francisco and Amazonia-West Africa (the so-called "Atlantica" cratons), during the Nuna cycle. Atlantica cratons are reconstructed within Nuna so that southwest Congo was adjacent to the northern Anabar shield of the Siberia craton at 1500 Ma. In this configuration, the ca. 1500 Ma LIPs of both cratons are proximal to each other. Considering the new 1385 Ma Virei pole, a distinct reconstruction is obtained such that southwest Congo lay close to the northwest West African craton. This requires a substantial transform motion and large-magnitude azimuthal rotation (~85°) of Congo-São Francisco between 1500 Ma and 1385 Ma, which could be related to early stages of the Nuna break-up. It also requires a large ca. 180° rotation of Congo-São Francisco relative to Laurentia, between 1385 Ma and the Neoproterozoic assembly of Rodinia.

CRediT authorship contribution statement

Johanna Salminen: Writing – original draft, Resources, Funding acquisition, Formal analysis, Data curation, Conceptualization. **David A.D. Evans:** Writing – review & editing, Investigation, Conceptualization, Funding aquisition, Resources. **Ricardo I.F. Trindade:** Writing – review & editing, Investigation, Conceptualization. **Richard Hanson:** Writing – review & editing, Resources. **Ulf Söderlund:** Writing – review & editing, Formal analysis. **Richard E. Ernst:** Writing – review & editing, Resources. **Martin B. Klausen:** Writing – review & editing, Investigation, Funding acquisition, Formal analysis. **Ian Fieldhouse:** Investigation.

Declaration of competing interest

The authors declare the following financial interests/personal relationships which may be considered as potential competing interests: Johanna Salminen reports financial support was provided by Research Council of Finland. Martin Klausen reports financial support was provided by National Research Foundation. David Evans reports financial support was provided by Pulse of the Earth. If there are other authors, they declare that they have no known competing financial interests or personal relationships that could have appeared to influence the work reported in this paper..

Data availability

Data will be made available on request.

Acknowledgements

We thank two anonymous reviewers for their suggestions and corrections which improved the manuscript. Authors are grateful for Jakes Smits, Manoel Sousa, Martin Bremer, and Fila Montagne for taking care of logistics during the field campaigns. Lakshika Palamakumbure is thanked for doing thermomagnetic measurements at the GTK. We thank Elisa Piispa for the insightful discussion. JS was funded by the Academy of Finland Research Fellow grant. MBK's sampling and geochemical analysis was funded by NRF (CSUR13082831396) and Anglo American. DE was funded by Yale University and U-Pb geochronology was funded by the Canadian NSERC grant CRDPJ 523131-17 (PI: REE) as part of the LIPs Industry-Academic Consortium (www.supercontinent.org). This is #0019 HelLabs publication.

References

Abbott, G., 1997. Geology of the upper Hart river area, eastern Ogilvie mountains, Yukon territory (116A/10, 116A/11): Yukon, indian and NorthernAffairs Canada. Exploration and Geological Services Division, Yukon, Indian and Northern Affairs Canada, Bulletin 9, 92p.

Abrahamsen, N., Van Der Voo, R., 1987. Palaeomagnetism of middle Proterozoic (c. 1.25 Ga) dykes from central North Greenland. Geophys. J. Int. 91, 597–611. https://doi.org/10.1111/j.1365-246X.1987.tb01660.x.

Abrajevitch, A., Van der Voo, R., 2010. Incompatible Ediacaran paleomagnetic directions suggest an equatorial geomagnetic dipole hypothesis. Earth Planet. Sci. Lett. 293, 164–170. https://doi.org/10.1016/j.epsl.2010.02.038.

Amelin, Y.V., Heaman, L.M., Verchogliad, V.M., Skobelev, V.M., 1994. Geochronological constraints on the emplacement history of an anorthosite — rapakivi granite suite: U−Pb zircon and baddeleyite study of the Korosten complex, Ukraine. Contrib. Miner. Petrol. 116, 411–419. https://doi.org/10.1007/BF00310908.

Ashwal, L.D., 1993. Anorthosites. Springer-Verlag, Berlin Heidelberg, Berlin, Heidelberg, New York, London, Paris, Tokyo, Hong Kong, p. 422.

Bispo-Santos, F., D'Agrella-Filho, M.S., Pacca, I.I.G., Janikian, L., Trindade, R.I.F., Elming, S.-A., Silva, J.A., Barros, M.A.S., Pinho, F.E.C., 2008. Columbia revisited: Paleomagnetic results from the 1790 Ma colider volcanics (SW Amazonian Craton, Brazil). Precambr. Res. 164, 40–49. https://doi.org/10.1016/j.precamres.2008.03.004.

Bispo-Santos, F., D'Agrella-Filho, M.S., Trindade, R.I.F., Elming, S.-Å., Janikian, L., Vasconcelos, P.M., Perillo, B.M., Pacca, I.I.G., da Silva, J.A., Barros, M.A.S., 2012. Tectonic implications of the 1419 Ma Nova Guarita mafic intrusives paleomagnetic pole (Amazonian Craton) on the longevity of Nuna. Precambr. Res. 196–197, 1–22. https://doi.org/10.1016/j.precamres.2011.10.022.

Bispo-Santos, F., D'Agrella-Filho, M.S., Trindade, R.I.F., Janikian, L., Reis, N.J., 2014. Was there SAMBA in Columbia? Paleomagnetic evidence from 1790 Ma Avanavero mafic sills (northern Amazonian Craton). Precambr. Res. 244, 139–155. https://doi.org/10.1016/j.precamres.2013.11.002.

Bispo-Santos, F., D'Agrella-Filho, M.S., Pesonen, L.J., Salminen, J.M., Reis, N.J., Silva, J. M., 2020. The long life of SAMBA connection in Columbia: A paleomagnetic study of the 1535 Ma Mucajaí complex, northern Amazonian Craton, Brazil. Gondw. Res. 80, 285–302. https://doi.org/10.1016/j.gr.2019.09.016.

Bleeker, W., 2003. The late Archean record: a puzzle in ca. 35 pieces. Lithos 71, 99–134. https://doi.org/10.1016/j.lithos.2003.07.003.

Bleeker, W., Ernst, R.E., 2006. Short-lived mantle generated magmatic events and their dyke swarms: The key unlocking Earth's paleogeographic record back to 2.6 Ga. In: Hanski, E., Mertanen, S., Rämö, T., Vuollo, J. (Eds.), Dyke Swarms—Time Markers of Crustal Evolution, pp.1-21.

Buchan, K.L., 2014. Reprint of "key paleomagnetic poles and their use in Proterozoic continent and supercontinent reconstructions: A review". Precambr. Res. 244, 5–22. https://doi.org/10.1016/j.precamres.2014.01.010.

Buchan, K.L., Halls, H.C., 1990. Paleomagnetism of proterozoicmafic dyke swarms of the Canadian shield. In: Parker, A.J., Rickwood, P.C., Tucker, D.H. (Eds.), Mafic Dykes and Emplacement Mechanisms. Balkema, Rotterdam, pp. 209–230.

Buchan, K.L., Mertanen, S., Park, R.G., Pesonen, L.J., Elming, S.Å., Abrahamsen, N., Bylund, G., 2000. Comparing the drift of Laurentia and Baltica in the Proterozoic: the importance of key palaeomagnetic poles. Tectonophysics 319, 167–198. https://doi.org/10.1016/S0040-1951(00)00032-9.

Bybee, G.M., Hayes, B., Owen-Smith, T.M., Lehmann, J., Ashwal, L.D., Brower, A.M., Hill, C.M., Corfu, F., Manga, M., 2019. Proterozoic massif-type anorthosites as the archetypes of long-lived (≥100 myr) magmatic systems—New evidence from the Kunene Anorthosite complex (Angola). Precambr. Res. 332, 105393 https://doi.org/10.1016/j.precamres.2019.105393.

Cederberg, J., Söderlund, U., Oliveira, E.P., Ernst, R.E., Pisarevsky, S.A., 2016. U-Pb baddeleyite dating of the proterozoic Pará de Minas dyke swarm in the São Francisco craton (Brazil) – implications for tectonic correlation with the siberian, Congo and North China cratons. Geologiska Föreningen 138, 219–240. https://doi.org/10.1080/11035897.2015.1093543.

Chadima, M., Hrouda, F., 2012. Cureval 8.0.2: Thermomagnetic Curve. Analyser for Windows, Agico, Inc.

Chaves, A.d.O., Rezende, C.R.d., 2019. Fragments of 1.79-1.75 Ga Large igneous provinces in reconstructing Columbia (Nuna): a Statherian supercontinent-superplume coupling? Episodes 42, 55–67. https://doi.org/10.18814/epiiugs/2019/019006.

Chen, L., Huang, B., Yi, Z., Zhao, J., Yan, Y., 2013. Paleomagnetism of ca. 1.35 Ga sills in northern North China craton and implications for paleogeographic reconstruction of the Mesoproterozoic supercontinent. Precambr. Res. 228, 36–47. https://doi.org/10.1016/j.precamres.2013.01.011.

Collins, A.S., Pisarevsky, S.A., 2005. Amalgamating eastern Gondwana: The evolution of the Circum-Indian Orogens. Earth Sci. Rev. 71, 229–270. https://doi.org/10.1016/j.earscirev.2005.02.004.

Condie, K., Pisarevsky, S.A., Korenaga, J., Gardoll, S., 2015. Is the rate of supercontinent assembly changing with time? Precambr. Res. 259, 278–289. https://doi.org/10.1016/j.precamres.2014.07.015.

D'Agrella-Filho, M.S., Trindade, R.I.F., Tohver, E., Janikian, L., Teixeira, W., Hall, C., 2011. Paleomagnetism and 40Ar/39Ar geochronology of the high-grade metamorphic rocks of the Jequié block, São Francisco craton: Atlantica, Ur and beyond. Precambr. Res. 185, 183–201. https://doi.org/10.1016/j.precamres.2011.01.008.

D'Agrella-Filho, M.S., Trindade, R.I.F., Queiroz, M.V.B., Meira, V.T., Janikian, L., Ruiz, A.S., Bispo-Santos, F., 2016. Reassessment of Aguapeí (Salto do Céu) paleomagnetic pole, Amazonian Craton and implications for Proterozoic supercontinents. Precambr. Res. 272, 1–17. https://doi.org/10.1016/j.precamres.2015.10.021.

D'Agrella-Filho, M.S., Trindade, R.I.F., Elming, S.-Å., Teixeira, W., Yokoyama, E., Tohver, E., Geraldes, M.C., Pacca, I.I.G., Barros, M.A.S., Ruiz, A.S., 2012. The 1420 Ma Indiavaí mafic intrusion (SW Amazonian Craton): Paleomagnetic results and implications for the Columbia supercontinent. Gondw. Res. 22, 956–973. https://doi.org/10.1016/j.gr.2012.02.022.

D'Agrella-Filho, M.S., Bispo-Santos, F., Trindade, R.I.F., Antonio, P.Y.J., 2016. Paleomagnetism of the Amazonian Craton and its role in paleocontinents. Brazilian J. Geol. 46.

D'Agrella-Filho, M.S., Teixeira, W., da Trindade, R.I.F., Patroni, O.A.L., Prieto, R.F., 2020. Paleomagnetism of 1.79 Ga Pará de Minas mafic dykes: testing a São Francisco/Congo-North China-Rio de la Plata connection in Columbia. Precambr. Res. 338 https://doi.org/10.1016/j.precamres.2019.105584.

de Kock, M.O., Gumsley, A.P., Klausen, M.B., Söderlund, U., Djeutchou, C., 2019. The Precambrian Mafic Magmatic Record, Including Large Igneous Provinces of the Kalahari Craton and Its Constituents: A Paleogeographic Review. In: Srivastava, R.K., Ernst, R.E., Peng, P. (Eds.), Dyke Swarms of the World: A Modern Perspective. Springer Singapore, Singapore, pp.155-214.10.1007/978-981-13-1666-1_5.

De Waele, B., Johnson, S.P., Pisarevsky, S.A., 2008. Palaeoproterozoic to Neoproterozoic growth and evolution of the eastern Congo Craton: its role in the Rodinia puzzle. Precambr. Res. 160, 127–141. https://doi.org/10.1016/j.precamres.2007.04.020.

de Wit, M., Furnes, H., MacLennan, S., Doucouré, M., Schoene, B., Weckmann, U., Martinez, U., Bowring, S., 2018. Paleoarchean bedrock lithologies across the Makhonjwa Mountains of South Africa and Swaziland linked to geochemical, magnetic and tectonic data reveal early plate tectonic genes flanking subduction margins. Geosci. Front. 9, 603–665. https://doi.org/10.1016/j.gsf.2017.10.005.

Deenen, M.H.L., Langereis, C.G., van Hinsbergen, D.J.J., Biggin, A.J., 2011. Geomagnetic secular variation and the statistics of palaeomagnetic directions. Geophys. J. Int. 186, 509–520. https://doi.org/10.1111/j.1365-246X.2011.05050.x.

Dekkers, M.J., 1990. Magnetic monitoring of pyrhhotite alteration during thermal demagnetization. Geophys. Res. Lett. 17, 779–782.

Djeutchou, C., de Kock, M., Ernst, R.E., Ossa Ossa, F.G., Bekker, A., 2024. A review of the intraplate mafic magmatic record of the greater Congo craton. Earth Sci. Rev. 249, 104649 https://doi.org/10.1016/j.earscirev.2023.104649.

Drüppel, K., Littmann, S., Romer, R.L., Okrusch, M., 2007. Petrology and isotope geochemistry of the Mesoproterozoic anorthosite and related rocks of the Kunene intrusive complex, NW Namibia. Precambr. Res. 156, 1–31. https://doi.org/10.1016/j.precamres.2007.02.005.

Dunlop, D.J., 2014. High-temperature susceptibility of magnetite: a new pseudo-single-domain effect. Geophys. J. Int. 199, 707–716. https://doi.org/10.1093/gji/ggu247.

Eggins, S.M., 2003. Laser ablation ICP-MS analysis of geological materials Prepared as lithium borate glasses. Geostand. Newslett. 27, 147–162. https://doi.org/10.1111/j.1751-908X.2003.tb00642.x.

Elburg, M.A., Cawthorn, R.G., 2017. Source and evolution of the alkaline Pilanesberg Complex, South Africa. Chem. Geol. 455, 148–165. https://doi.org/10.1016/j.chemgeo.2016.10.007.

Elming, S.-Å., Salminen, J., Pesonen, L.J., 2021. Chapter 16 - Paleo-Mesoproterozoic Nuna supercycle. In: Pesonen, L.J., Salminen, J., Elming, S.-Å., Evans, D.A.D., Veikkolainen, T. (Eds.), Ancient Supercontinents and the Paleogeography of Earth. Elsevier, pp.499-548.DOI: 10.1016/B978-0-12-818533-9.00001-1.

Elming, S.Å., Moakhar, M.O., Layer, P., Donadini, F., 2009. Uplift deduced from remanent magnetization of a proterozoic basic dyke and the baked country rock in the Hoting area, Central Sweden: a palaeomagnetic and40Ar/39Ar study. Geophys. J. Int. 179, 59–78. https://doi.org/10.1111/j.1365-246X.2009.04265.x.

Elston, D.P., Enkin, R.J., Baker, J., Kisilevsky, D.K., 2002. Tightening the belt: paleomagnetic-stratigraphic constraints on deposition, correlation, and deformation of the Middle Proterozoic (ca. 1.4 Ga) Belt-Purcell supergroup, United States and Canada. Geol. Soc. Am. Bull. 114, 619–638. https://doi.org/10.1130/0016-7606(2002)114.

Emslie, R.F., Irving, E., Park, J.K., 1976. Further paleomagnetic results from the Michikamau Intrusion, Labrador. Can. J. Earth Sci. 13, 1052–1057. https://doi.org/10.1139/e76-108.
Ernst, R.E., Buchan, K.L., 2001. Large mafic magmatic events through time and links to mantle-plume heads. In: Ernst, R.E., Buchan, K.L. (Eds.), Mantle Plumes: Their Identification Through Time. Geological Society of America Special Paper, pp.483-575.
Ernst, R., Bleeker, W., 2010. Large igneous provinces (LIPs), giant dyke swarms, and mantle plumes: significance for breakup events within Canada and adjacent regions from 2.5 Ga to the present. Can. J. Earth Sci. 47, 695–739. https://doi.org/10.1139/E10-025.
Ernst, R.E., Buchan, K.L., Hamilton, M.A., Okrugin, A.V., Tomshin, M.D., 2000. Integrated Paleomagnetism and U-Pb Geochronology of mafic dikes of the eastern Anabar shield region, Siberia: implications for Mesoproterozoic Paleolatitude of Siberia and Comparison with Laurentia. J. Geol. 108, 381–401. https://doi.org/10.1086/314413.
Ernst, R.E., Bond, D.P.G., Zhang, S.-H., Buchan, K.L., Grasby, S.E., Youbi, N., El Bilali, H., Bekker, A., Doucet, L.S., 2021. Large Igneous Province Record Through Time and Implications for Secular Environmental Changes and Geological Time-Scale Boundaries. Large Igneous Provinces, pp.1-26.DOI: 10.1002/9781119507444.ch1.
Ernst, R.E., Pereira, E., Hamilton, M.A., Pisarevsky, S.A., Rodriques, J., Tassinari, C.C.G., Teixeira, W., Van-Dunem, V., 2013. Mesoproterozoic intraplate magmatic 'barcode' record of the Angola portion of the Congo Craton: Newly dated magmatic events at 1505 and 1110 Ma and implications for Nuna (Columbia) supercontinent reconstructions. Precambr. Res. 230, 103–118. https://doi.org/10.1016/j.precamres.2013.01.010.
Ernst, R.E., Hamilton, M.A., Söderlund, U., Hanes, J.A., Gladkochub, D.P., Okrugin, A.V., Kolotilina, T., Mekhonoshin, A.S., Bleeker, W., LeCheminant, A.N., Buchan, K.L., Chamberlain, K.R., Didenko, A.N., 2016. Long-lived connection between southern Siberia and northern Laurentia in the proterozoic. Nat. Geosci. 9, 464–469. https://doi.org/10.1038/ngeo2700.
Evans, D.A.D., 2003. True polar wander and supercontinents. Tectonophysics 362, 303–320. https://doi.org/10.1016/S0040-1951(02)000642-X.
Evans, D.A.D., 2009. The palaeomagnetically viable, long-lived and all-inclusive Rodinia supercontinent reconstruction. Geol. Soc. Lond. Spec. Publ. 327, 371–404. https://doi.org/10.1144/sp327.16.
Evans, D.A.D., 2013. Reconstructing pre-Pangean supercontinents. Geol. Soc. Am. Bull. 125, 1735–1751. https://doi.org/10.1130/b30950.1.
Evans, D.A.D., Pisarevsky, S.A., 2008. Plate tectonics on early Earth? Weighing the paleomagnetic evidence. Special Paper 440: When Did Plate Tectonics Begin on Planet Earth?, 249-263. doi: 10.1130/2008.2440(12).
Evans, D.A.D., Mitchell, R.N., 2011. Assembly and breakup of the core of Paleoproterozoic-Mesoproterozoic supercontinent Nuna. Geology 39, 443–446. https://doi.org/10.1130/G31654.1.
Evans, D.A.D., Veselovsky, R.V., Petrov, P.Y., Shatsillo, A.V., Pavlov, V.E., 2016. Paleomagnetism of mesoproterozoic margins of the Anabar shield: A hypothesized billion-year partnership of Siberia and northern Laurentia. Precambr. Res. 281, 639–655. https://doi.org/10.1016/j.precamres.2016.06.017.
Fisher, R., 1953. Dispersion of a sphere. Proc. R. Soc. Lond. 217, 295–305.
Franceschinis, P.R., Rapalini, A.E., Sánchez Bettucci, L., Martínez Dopico, C., Milanese, F. N., 2019. Paleomagnetic confirmation of the "unorthodox" configuration of Atlantica between 2.1 and 2.0 Ga. Precambr. Res. 334 https://doi.org/10.1016/j.precamres.2019.105447.
Gladkochub, D.P., Donskaya, T.V., Pisarevsky, S.A., Ernst, R.E., Söderlund, U., Kotov, A. B., Kovach, V.P., Okrugin, A.V., 2022. 1.79–1.75 Ga mafic magmatism of the Siberian craton and late Paleoproterozoic paleogeography. Precambr. Res. 370, 106557 https://doi.org/10.1016/j.precamres.2022.106557.
Gong, Z., Evans, D.A.D., Youbi, N., Lahna, A.A., Söderlund, U., Malek, M.A., Wen, B., Jing, X., Ding, J., Boumehdi, M.A., Ernst, R.E., 2021. Reorienting the West African craton in Paleoproterozoic-Mesoproterozoic supercontinent Nuna. Geology 49, 1171–1176. https://doi.org/10.1130/G48855.1.
Goscombe, B., Foster, D.A., Gray, D., Wade, B., 2018. The evolution of the Damara orogenic system: A record of West Gondwana assembly and crustal response. Geology of Southwest Gondwana 303–352. https://doi.org/10.1007/978-3-319-68920-3_12.
Gower, C.F., Ryan, A.F., Rivers, T., 1990. Mid-Proterozoic Laurentia-Baltica: an overview of its geological evolution and a summary of the contributions made by this volume. In: Gower C.F., Rivers T., Ryan B. (eds.), Mid Proterozoic Laurentia-Baltica. Geological Association of Canada, Special Paper 38, 1-20.
Halls, H.C., Li, J., Davis, D., Hou, G., Zhang, B., Qian, X., 2000. A precisely dated proterozoic palaeomagnetic pole from the North China craton, and its relevance to palaeocontinental reconstruction. Geophys. J. Int. 143, 185–203. https://doi.org/10.1046/j.1365-246x.2000.00231.x.
Hamilton, M.A., Buchan, K.L., 2010. U-Pb geochronology of the Western Channel diabase, northwestern Laurentia: implications for a large 1.59 Ga magmatic province, Laurentia's APWP and paleocontinental reconstructions of Laurentia, Baltica and Gawler craton of Southern Australia. Precambr. Res. 183, 463–473. https://doi.org/10.1016/j.precamres.2010.06.009.
Hanson, R.E., Harmer, R.E., Blenkinsop, T.G., Bullen, D.S., Dalziel, I.W.D., Gose, W.A., Hall, R.P., Kampunzu, A.B., Key, R.M., Mukwakwami, J., Munyanyiwa, H., Pancake, J.A., Seidel, E.K., Ward, S.E., 2006. Mesoproterozoic intraplate magmatism in the Kalahari Craton: A review. J. Afr. Earth Sc. 46, 141–167. https://doi.org/10.1016/j.jafrearsci.2006.01.016.
Hanson, R.E., 2003. Proterozoic geochronology and tectonic evolution of southern Africa. In: Yoshida, M., Windley, B.F., Dasgupta, S. (Eds.), Proterozoic East Gondwana: Supercontinent Assembly and Breakup. Geological Society of London, pp. 427-463. doi: 10.1144/GSL.SP.2003.206.01.20.
Heslop, D., Roberts, A.P., 2018. Revisiting the paleomagnetic reversal test: A Bayesian hypothesis testing framework for a common mean direction. J. Geophys. Res. Solid Earth 123, 7225–7236. https://doi.org/10.1029/2018JB016081.
Hurley, P.M., Rand, J.R., Pinson, W.H., Fairbairn, H.W., de Almeida, F.F.M., Melcher, G. C., Cordani, U.G., Kawashita, K., Vandoros, P., 1967. Test of continental drift by Comparison of radiometric ages. Science 157, 495–500. https://doi.org/10.1126/science.157.3788.495.
Idnurm, M., 2000. Towards a high resolution late Palaeoproterozoic - earliest Mesoproterozoic apparent polar wander path for northern Australia. Aust. J. Earth Sci. 47, 405–429. https://doi.org/10.1046/j.1440-0952.2000.00788.x.
Idnurm, M., Giddings, J.W., Plumb, K.A., 1995. Apparent polar wander and reversal stratigraphy of the palaeo-mesoproterozoic southeastern McArthur Basin, Australia. Precambr. Res. 72, 1–41.
Irving, E., 2004. Early proterozoic geomagnetic field in western Laurentia: implications for paleolatitudes, local rotations and stratigraphy. Precambr. Res. 129, 251–270. https://doi.org/10.1016/j.precamres.2003.10.002.
Irving, E., Donaldson, J.A., Park, J.K., 1972. Paleomagnetism of the Western Channel diabase and associated rocks, Northwest Territories. Can. J. Earth Sci. 9, 960–971. https://doi.org/10.1139/e72-080.
Jaffey, A.H., Flynn, K.F., Glendenin, L.E., Bentley, W.C., Essling, A.M., 1971. Precision measurement of half-lives and specific activities of ^{235}U and ^{238}U. Phys. Rev. C 4, 1889–1906. https://doi.org/10.1103/PhysRevC.4.1889.
Jelsma, H.A., McCourt, S., Perritt, S.H., Armstrong, R.A., 2018. The Geology and Evolution of the Angolan Shield, Congo Craton. In: Siegesmund, S., Basei, M.A.S., Oyhantçabal, P., Oriolo, S. (Eds.), Geology of Southwest Gondwana. Springer International Publishing, Cham, pp.217-239.10.1007/978-3-319-68920-3_9.
Johansson, Å., 2009. Baltica, Amazonia and the SAMBA connection—1000 million years of neighbourhood during the proterozoic? Precambr. Res. 175, 221–234. https://doi.org/10.1016/j.precamres.2009.09.011.
Johansson, Å., Bingen, B., Huhma, H., Waight, T., Vestergaard, R., Soesoo, A., Skridlaite, G., Krzeminska, E., Shumlyanskyy, L., Holland, M.E., Holm-Denoma, C., Teixeira, W., Faleiros, F.M., Ribeiro, B.V., Jacobs, J., Wang, C., Thomas, R.J., Macey, P.H., Kirkland, C.L., Hartnady, M.I.H., Eglington, B.M., Puetz, S.J., Condie, K. C., 2022. A geochronological review of magmatism along the external margin of Columbia and in the Grenville-age orogens forming the core of rodinia. Precambr. Res. 371, 106463 https://doi.org/10.1016/j.precamres.2021.106463.
Johnson, C.L., Constable, C.G., Tauxe, L., Barendregt, R., Brown, L.L., Coe, R.S., Layer, P., Mejia, V., Opdyke, N.D., Singer, B.S., Staudigel, H., Stone, D.B., 2008. Recent investigations of the 0–5 Ma geomagnetic field recorded by lava flows. Geochem. Geophys. Geosyst. 9 https://doi.org/10.1029/2007GC001696.
Jones, C.H., 2002. User-driven integrated software lives: "Paleomag" paleomagnetics analysis on the Macintosh. Comput. Geosci. 28, 1145–1151. https://doi.org/10.1016/S0098-3004(02)00032-8.
Kirscher, U., Liu, Y., Li, Z.X., Mitchell, R.N., Pisarevsky, S.A., Denyszyn, S.W., Nordsvan, A., 2019. Paleomagnetism of the Hart dolerite (Kimberley, Western Australia) – A two-stage assembly of the supercontinent Nuna? Precambr. Res. 329, 170–181. https://doi.org/10.1016/j.precamres.2018.12.026.
Kirscher, U., Mitchell, R.N., Liu, Y., Nordsvan, A.R., Cox, G.M., Pisarevsky, S.A., Wang, C., Wu, L., Murphy, J.B., Li, Z.-X., 2020. Paleomagnetic constraints on the duration of the Australia-Laurentia connection in the core of the Nuna supercontinent. Geology 49, 174–179. https://doi.org/10.1130/G47823.1.
Kirschvink, J.L., 1980. The least-squares line and plane and the paleomagnetic data. Geophysical Journal of the Royal Astronomy Society 62, 699–718.
Kirschvink, J.L., Kopp, R.E., Raub, T.D., Baumgartner, C.T., Holt, J.W., 2008. Rapid, precise, and high-sensitivity acquisition of paleomagnetic and rock-magnetic data: Development of a low-noise automatic sample changing system for superconducting rock magnetometers. Geochem. Geophys. Geosyst. 9, n/a-n/a. https://doi.org/10.1029/2007gc001856.
Klausen, M.B., Szilas, K., Kokfelt, T.F., Keulen, N., Schumacher, J.C., Berger, A., 2017. Tholeiitic to calc-alkaline metavolcanic transition in the Archean Nigerlikasik Supracrustal Belt, SW Greenland. Precambr. Res. 302, 50–73. https://doi.org/10.1016/j.precamres.2017.09.014.
Kokonyangi, J.W., Kampunzu, A.B., Armstrong, R., Yoshida, M., Okudaira, T., Arima, M., Ngulube, D.A., 2006. The Mesoproterozoic Kibaride belt (Katanga, SE D.R. Congo). J. Afr. Earth Sc. 46, 1–35. https://doi.org/10.1016/j.jafrearsci.2006.01.017.
Kröner, A., Rojas-Agramonte, Y., 2017. Mesoproterozoic (Grenville-age) granitoids and supracrustal rocks in kaokoland, northwestern Namibia. Precambr. Res. 298, 572–592. https://doi.org/10.1016/j.precamres.2017.07.008.
Larson, T., 2015. Mesoproterozoic paleomagnetism of the southern Congo craton. Yale University, Department of Geology and Geophysics, p. 79.
Lehmann, J., Bybee, G.M., Hayes, B., Owen-Smith, T.M., Belyanin, G., 2020. Emplacement of the giant Kunene AMCG complex into a contractional ductile shear zone and implications for the Mesoproterozoic tectonic evolution of SW Angola. Int. J. Earth Sci. 109, 1463–1485. https://doi.org/10.1007/s00531-020-01837-5.
Li, Z.-X., Evans, D.A.D., 2011. Late neoproterozoic 40° intraplate rotation within Australia allows for a tighter-fitting and longer-lasting Rodinia. Geology 39, 39–42. https://doi.org/10.1130/G31461.1.
Li, Z.-X., Liu, Y., Ernst, R., 2023. A dynamic 2000–540 ma Earth history: from cratonic amalgamation to the age of supercontinent cycle. Earth Sci. Rev. 238, 104336 https://doi.org/10.1016/j.earscirev.2023.104336.
Lovecchio, J.P., Rohais, S., Joseph, P., Bolatti, N.D., Ramos, V.A., 2020. Mesozoic rifting evolution of SW Gondwana: A poly-phased, subduction-related, extensional history responsible for basin formation along the argentinean Atlantic margin. Earth Sci. Rev. 203, 103138 https://doi.org/10.1016/j.earscirev.2020.103138.

Lubnina, N.V., 2009. The East European Craton in the Mesoproterozoic: New key paleomagnetic poles. Dokl. Earth Sci. 428, 1174–1178. https://doi.org/10.1134/s1028334x09070307.
Ludwig, K.R., 2003. User's Manual for Isoplot 3.00 : A Geochronological Toolkit for Microsoft Excel. Revised August 27, 2003. ed, Berkeley CA .
Luoto, T., Salminen, J., Obst, K., 2021. Revisiting mafic dykes of Bornholm – Implications for Baltica in supercontinent Nuna at 1.3 Ga. Precambr. Res. 367, 106444 https://doi.org/10.1016/j.precamres.2021.106444.
Macgregor, D., 2018. History of the development of permian-cretaceous rifts in East Africa: A series of interpreted maps through time. Pet. Geosci. 24, 8–20. https://doi.org/10.1144/petgeo2016-155.
Maier, W.D., Rasmussen, B., Fletcher, I.R., Li, C., Barnes, S.J., Huhma, H., 2013. The Kunene Anorthosite complex, Namibia, and its satellite intrusions: geochemistry, geochronology, and economic potential. Econ. Geol. 108, 953–986. https://doi.org/10.2113/econgeo.108.5.953.
Mäkitie, H., Data, G., Isabirye, E., Mänttäri, I., Huhma, H., Klausen, M.B., Pakkanen, L., Virransalo, P., 2014. Petrology, geochronology and emplacement model of the giant 1.37Ga arcuate Lake Victoria Dyke Swarm on the margin of a large igneous province in eastern Africa. J. Afr. Earth Sc. 97, 273–296. https://doi.org/10.1016/j.jafrearsci.2014.04.034.
Malyshev, S.V., Pasenko, A.M., Ivanov, A.V., Gladkochub, D.P., Savatenkov, V.M., Meffre, S., Abersteiner, A., Kamenetsky, V.S., Shcherbakov, V.D., 2018. Geodynamic significance of the mesoproterozoic magmatism of the udzha paleo-rift (Northern Siberian craton) based on U-Pb geochronology and paleomagnetic data. Minerals 8, 555. https://doi.org/10.3390/min8120555.
Marcussen, C., Abrahamsen, N., 1983. Palaeomagnetism of the proterozoic zig-Zag dal basalt and the Midsommersø dolerites, eastern North Greenland. Geophys. J. Int. 73, 367–387. https://doi.org/10.1111/j.1365-246X.1983.tb03321.x.
Mayer, A., Hofmann, A.W., Sinigoi, S., Morais, E., 2004. Mesoproterozoic Sm–Nd and U-Pb ages for the Kunene Anorthosite complex of SW Angola. Precambr. Res. 133, 187–206. https://doi.org/10.1016/j.precamres.2004.04.003.
McCourt, S., Armstrong, R.A., Jelsma, H., Mapeo, R.B.M., 2013. New U-pb SHRIMP ages from the Lubango region, SW Angola: insights into the palaeoproterozoic evolution of the Angolan Shield, southern Congo Craton, Africa. J. Geol. Soc. London 170, 353–363. https://doi.org/10.1144/jgs2012-059.
McElhinny, M.W., Powell, C.M., Pisarevsky, S.A., 2003. Paleozoic terranes of eastern Australia and the drift history of Gondwana. Tectonophysics 362, 41–65. https://doi.org/10.1016/s0040-1951(02)00630-3.
McFadden, P.L., Lowes, F.J., 1981. The discrimination of mean directions drawn from Fisher distributions. Geophys. J. Int. 67, 19–33. https://doi.org/10.1111/j.1365-246X.1981.tb02729.x.
McFadden, P.L., McElhinny, M.W., 1990. Classification of the reversal test in palaeomagnetism. Geophys. J. Int. 103, 725–729. https://doi.org/10.1111/j.1365-246X.1990.tb05683.x.
Meert, J.G., Hargraves, R.B., Van der Voo, R., Hall, C.M., Halliday, A.N., 1994. Paleomagnetic and 40Ar/39Ar studies of late Kibaran intrusives in Burundi, East Africa: Implications for Late Proterozoic Supercontinents. J. Geol. 102, 621–637. https://doi.org/10.1086/629708.
Meert, J.G., Stuckey, W., 2002. Revisiting the paleomagnetism of the 1.476 Ga st. Francois mountains igneous province, Missouri, 1–1-1-19 Tectonics 21. https://doi.org/10.1029/2000tc001265.
Meert, J.G., Pivarunas, A.F., Evans, D.A.D., Pisarevsky, S.A., Pesonen, L.J., Li, Z.-X., Elming, S.-Å., Miller, S.R., Zhang, S., Salminen, J.M., 2020. The magnificent seven: A proposal for modest revision of the Van der voo (1990) quality index. Tectonophysics 790, 228549. https://doi.org/10.1016/j.tecto.2020.228549.
Milani, L., Lehmann, J., Bybee, G.M., Hayes, B., Owen-Smith, T.M., Oosthuizen, L., Delport, P.W.J., Ueckermann, H., 2022. Geochemical and geochronological constraints on the Mesoproterozoic Red Granite Suite, Kunene AMCG complex of Angola and Namibia. Precambr. Res. 379, 106821 https://doi.org/10.1016/j.precamres.2022.106821.
Mitchell, R.N., Zhang, N., Salminen, J., Liu, Y., Spencer, C.J., Steinberger, B., Murphy, J. B., Li, Z.-X., 2021. The supercontinent cycle. Nature Reviews Earth & Environment 2, 358–374. https://doi.org/10.1038/s43017-021-00160-0.
Müller, R.D., Seton, M., Zahirovic, S., Williams, S.E., Matthews, K.J., Wright, N.M., Shephard, G.E., Maloney, K.T., Barnett-Moore, N., Hosseinpour, M., Bower, D.J., Cannon, J., 2016. Ocean Basin evolution and global-scale plate reorganization events since Pangea breakup. Annu. Rev. Earth Planet. Sci. 44, 107–138. https://doi.org/10.1146/annurev-earth-060115-012211.
Müller, R.D., Zahirovic, S., Williams, S.E., Cannon, J., Seton, M., Bower, D.J., Tetley, M. G., Heine, C., Le Breton, E., Liu, S., Russell, S.H.J., Yang, T., Leonard, J., Gurnis, M., 2019. A global plate model including lithospheric deformation along major rifts and orogens since the Triassic. Tectonics 38, 1884–1907. https://doi.org/10.1029/2018tc005462.
Nance, R.D., Murphy, J.B., Santosh, M., 2014. The supercontinent cycle: A retrospective essay. Gondw. Res. 25, 4–29. https://doi.org/10.1016/j.gr.2012.12.026.
Neres, M., Silva, P.F., Ikenne, M., Martins, S., Hafid, A., Mata, J., Almeida, F., Youbi, N., Boumehdi, M.A., 2016. Evidences for multiple remagnetization of proterozoic dykes from iguerda inlier (Anti-Atlas Belt, Southern Morocco). Stud. Geophys. Geod. 60, 700–730. https://doi.org/10.1007/s11200-014-0178-x.
Owens, B.E., Dymek, R.F., 2001. Petrogenesis of the labrieville alkalic Anorthosite Massif, Grenville Province, Quebec. J. Petrol. 42, 1519–1546. https://doi.org/10.1093/petrology/42.8.1519.
Palmer, H.C., 1970. Paleomagnetism and correlation of some Middle Keweenawan rocks, Lake Superior. Can. J. Earth Sci. 7, 1410–1436. https://doi.org/10.1139/e70-136.
Panzik, J.E., Evans, D.A.D., 2014. Assessing the GAD hypothesis with paleomagnetic data from large proterozoic dike swarms. Earth Planet. Sci. Lett. 406, 134–141. https://doi.org/10.1016/j.epsl.2014.09.007.
Park, J.K., Irving, E., Donaldson, J.A., 1973. Paleomagnetism of the Precambrian Dubawnt Group. Geol. Soc. Am. Bull. 84, 859–870.
Pearce, J., 1996. A user's guide to basalt discrimination diagrams. In: Wyman, D.A. (Ed.), Trace Element Geochemistry of Volcanic Rocks: Applications for Massive Sulphide Exploration. Geological Association of Canada, Short Course Notes, pp. 79–113.
Pearce, J., Ernst, R., Peate, D., Rogers, C., 2021. LIP printing: Use of immobile element proxies to characterize Large Igneous Provinces in the geologic record. Lithos 392–393, 106068. https://doi.org/10.1016/j.lithos.2021.106068.
Pehrsson, S.J., Eglington, B.M., Evans, D.A.D., Huston, D., Reddy, S.M., 2016. Metallogeny and its link to orogenic style during the Nuna supercontinent cycle. Geol. Soc. Lond. Spec. Publ. 424, 83–94. https://doi.org/10.1144/sp424.5.
Pei, J., Yang, Z., Zhao, Y., 2006. A Mesoproterozoic paleomagnetic pole from the Yangzhuang formation, North China and its tectonics implications. Precambr. Res. 151, 1–13. https://doi.org/10.1016/j.precamres.2006.06.001.
Pesonen, L.J., Nevanlinna, H., 1981. Late Precambrian Keweenawan asymmetric reversals. Nature 294, 436–439. https://doi.org/10.1038/294436a0.
Pesonen, L.J., Elming, S.Å., Mertanen, S., Pisarevsky, S., D'Agrella-Filho, M.S., Meert, J. G., Schmidt, P.W., Abrahamsen, N., Bylund, G., 2003. Palaeomagnetic configuration of continents during the Proterozoic. Tectonophysics 375, 289–324. https://doi.org/10.1016/s0040-1951(03)00343-3.
Pesonen, L.J., Mertanen, S., Veikolainen, T., 2012. Paleo-mesoproterozoic supercontinents - A paleomagnetic view. Geophysica 48, 5–47.
Piper, J.D.A., 1974. Magnetic properties of the Cunene Anorthosite complex, Angola. Phys. Earth Planet. In. 9, 353–363. https://doi.org/10.1016/0031-9201(74)90063-6.
Pisarevsky, S.A., Bylund, G., 2011. Paleomagnetism of 1780–1770 Ma mafic and composite intrusions of Smaland (Sweden): Implications for the mesoproterozoic supercontinent. Am. J. Sci. 310, 1168–1186. https://doi.org/10.2475/09.2010.15.
Pisarevsky, S.A., Sokolov, S.J., 2001. The magnetostratigraphy and a 1780 Ma palaeomagnetic pole from the red sandstones of the Vazhinka River section, Karelia, Russia. Geophys. J. Int. 146, 531–538. https://doi.org/10.1046/j.0956-540x.2001.01479.x.
Pisarevsky, S.A., Natapov, L.M., Donskaya, T.V., Gladkochub, D.P., Vernikovsky, V.A., 2008. Proterozoic Siberia: A promontory of Rodinia. Precambr. Res. 160, 66–76. https://doi.org/10.1016/j.precamres.2007.04.016.
Pisarevsky, S.A., Elming, S.-Å., Pesonen, L.J., Li, Z.-X., 2014. Mesoproterozoic paleogeography: Supercontinent and beyond. Precambr. Res. 244, 207–225. https://doi.org/10.1016/j.precamres.2013.05.014.
Porada, H., 1989. Pan-African rifting and orogenesis in southern to equatorial Africa and eastern Brazil. Precambr. Res. 44, 103–136. https://doi.org/10.1016/0301-9268(89)90078-8.
Puchkov, V.N., Bogdanova, S.V., Ernst, R.E., Kozlov, V.I., Krasnobaev, A.A., Söderlund, U., Wingate, M.T.D., Postnikov, A.V., Sergeeva, N.D., 2013. The ca. 1380 Ma Mashak igneous event of the Southern Urals. Lithos 174, 109–124. https://doi.org/10.1016/j.lithos.2012.08.021.
Rapalini, A.E., Franceschinis, P.R., Bettucci, L.S., Arrouy, M.J., Poiré, D.G., 2021. Chapter 7 - The Precambrian drift history and paleogeography of Río de la Plata craton. In: Pesonen, L.J., Salminen, J., Elming, S.-Å., Evans, D.A.D., Veikkolainen, T. (Eds.), Ancient Supercontinents and the Paleogeography of Earth. Elsevier, pp.243-261.DOI: 10.1016/B978-0-12-818533-9.00002-3.
Rapalini, A.E., Sánchez Bettucci, L., Badgen, E., Vásquez, C.A., 2015. Paleomagnetic study on mid-Paleoproterozoic rocks from the Rio de la Plata craton: Implications for Atlantica. Gondw. Res. 27, 1534–1549. https://doi.org/10.1016/j.gr.2014.01.012.
Roest, W.R., Srivastava, S.P., 1989. Sea-floor spreading in the Labrador Sea: A new reconstruction. Geology 17, 1000–1003. https://doi.org/10.1130/0091-7613(1989)017<1000:SFSITL>2.3.CO;2.
Rogers, J.J.W., 1996. A History of Continents in the past Three Billion Years. 104, 91–107. https://doi.org/10.1086/629803.
Rogers, J.J.W., Santosh, M., 2009. Tectonics and surface effects of the supercontinent Columbia. Gondw. Res. 15, 373–380. https://doi.org/10.1016/j.gr.2008.06.008.
Salminen, J., Pesonen, L.J., Mertanen, S., Vuollo, J., Airo, M.L., 2009. Palaeomagnetism of the Salla Diabase dyke, northeastern Finland, and its implication for the Baltica-Laurentia entity during the Mesoproterozoic. Geol. Soc. Lond. Spec. Publ. 323, 199–217. https://doi.org/10.1144/sp323.9.
Salminen, J., Mertanen, S., Evans, D.A.D., Wang, Z., 2014. Paleomagnetic and geochemical studies of the mesoproterozoic Satakunta dyke swarms, Finland, with implications for a Northern Europe – North America (NENA) connection within Nuna supercontinent. Precambr. Res. 244, 170–191. https://doi.org/10.1016/j.precamres.2013.08.006.
Salminen, J., Evans, D.A.D., Trindade, R.I.F., Oliveira, E.P., Piispa, E.J., Smirnov, A.V., 2016a. Paleogeography of the congo/São Francisco craton at 1.5Ga: expanding the core of nuna supercontinent. Precambr. Res. 286, 195–212. https://doi.org/10.1016/j.precamres.2016.09.011.
Salminen, J., Klein, R., Mertanen, S., Pesonen, L.J., Fröjdö, S., Mänttäri, I., Eklund, O., 2016b. Palaeomagnetism and U-Pb geochronology of c. 1570 Ma intrusives from åland archipelago, SW Finland – implications for Nuna. Geol. Soc. Lond. Spec. Publ. 424, 95–118. https://doi.org/10.1144/sp424.3.
Salminen, J., Hanson, R., Evans, D.A.D., Gong, Z., Larson, T., Walker, O., Gumsley, A., Söderlund, U., Ernst, R., 2018. Direct Mesoproterozoic connection of the Congo and Kalahari cratons in proto-Africa: Strange attractors across supercontinental cycles. Geology 46, 1011–1014. https://doi.org/10.1130/g45294.1.
Salminen, J., Elming, S.-Å., Mertanen, S., Wang, C., Almqvist, B., Moakhar, M.O., 2021. Paleomagnetic studies of rapakivi complexes in the Fennoscandian shield –

implications to the origin of Proterozoic massif-type anorthosite magmatism. Precambr. Res. 365, 106406 https://doi.org/10.1016/j.precamres.2021.106406.
Salminen, J., Pesonen, L., 2007. Paleomagnetic and rock magnetic study of the Mesoproterozoic sill, Valaam island, Russian Karelia. Precambr. Res. 159, 212–230. https://doi.org/10.1016/j.precamres.2007.06.009.
Scherbak, D.P., Ponomarenko, A.N., Makarenko, I.D., 1995. Geochronology of the granites from the ingulo-ingulets block of the Ukrainian shield, geochemistry and ore origin. Naukova Dumka 21, 74–88 in Russian.
Schmidt, P.W., 1993. Palaeomagnetic cleaning strategies. Phys. Earth Planet. In. 76, 169–178. https://doi.org/10.1016/0031-9201(93)90066-I.
Schmidt, P.W., Williams, G.E., 2008. Palaeomagnetism of red beds from the Kimberley group, Western Australia: Implications for the palaeogeography of the 1.8 Ga King Leopold glaciation. Precambr. Res. 167, 267–280. https://doi.org/10.1016/j.precamres.2008.09.002.
Shumlyanskyy, L., Ernst, R.E., Albekov, A., Söderlund, U., Wilde, S.A., Bekker, A., 2021. The early statherian (ca. 1800–1750 Ma) Prutivka-Novogol large igneous province of Sarmatia: Geochronology and implication for the Nuna/Columbia supercontinent reconstruction. Precambr. Res. 358, 106185 https://doi.org/10.1016/j.precamres.2021.106185.
Silveira, E.M., Söderlund, U., Oliveira, E.P., Ernst, R.E., Leal, A.B.M., 2013. First precise U-pb baddeleyite ages of 1500Ma mafic dykes from the São Francisco craton, Brazil, and tectonic implications. Lithos 174, 144–156. https://doi.org/10.1016/j.lithos.2012.06.004.
Söderlund, U., Johansson, L., 2002. A simple way to extract baddeleyite (ZrO2), 1 of 7–7 of 7 Geochem. Geophys. Geosyst. 3. https://doi.org/10.1029/2001GC000212.
Stacey, J.S., Kramers, J.D., 1975. Approximation of terrestrial lead isotope evolution by a two-stage model. Earth Planet. Sci. Lett. 26, 207–221. https://doi.org/10.1016/0012-821X(75)90088-6.
Stark, J.C., Wang, X.-C., Li, Z.-X., Denyszyn, S.W., Rasmussen, B., Zi, J.-W., 2018. 1.39 Ga mafic dyke swarm in southwestern Yilgarn Craton marks Nuna to Rodinia transition in the West Australian Craton. Precambr. Res. 316, 291–304. https://doi.org/10.1016/j.precamres.2018.08.014.
Steiger, R.H., Jäger, E., 1977. Subcommission on geochronology: Convention on the use of decay constants in geo- and cosmochronology. Earth Planet. Sci. Lett. 36, 359–362. https://doi.org/10.1016/0012-821X(77)90060-7.
Swanson-Hysell, N.L., Vaughan, A.A., Mustain, M.R., Asp, K.E., 2014. Confirmation of progressive plate motion during the Midcontinent Rift's early magmatic stage from the Osler Volcanic Group, Ontario, Canada. Geochem. Geophys. Geosyst. 15, 2039–2047. https://doi.org/10.1002/2013gc005180.
Tack, L., Wingate, M.T.D., De Waele, B., Meert, J., Belousova, E., Griffin, B., Tahon, A., Fernandez-Alonso, M., 2010. The 1375 Ma "Kibaran event" in Central Africa: prominent emplacement of bimodal magmatism under extensional regime. Precambr. Res. 180, 63–84. https://doi.org/10.1016/j.precamres.2010.02.022.
Tanaka, H., Idnurm, M., 1994. Palaeomagnetism of proterozoic mafic intrusions and host rocks of the Mount Isa inlier, Australia: revisited. Precambr. Res. 69, 241–258. https://doi.org/10.1016/0301-9268(94)90089-2.
Teixeira, W., Hamilton, M.A., Girardi, V.A.V., Faleiros, F.M., Ernst, R.E., 2019. U-pb baddeleyite ages of key dyke swarms in the Amazonian Craton (Carajás/Rio Maria and rio apa areas): Tectonic implications for events at 1880, 1110 Ma, 535 Ma and 200 Ma. Precambr. Res. 329, 138–155. https://doi.org/10.1016/j.precamres.2018.02.008.
Thompson, J.O., Moulin, M., Aslanian, D., de Clarens, P., Guillocheau, F., 2019. New starting point for the Indian Ocean: Second phase of breakup for Gondwana. Earth Sci. Rev. 191, 26–56. https://doi.org/10.1016/j.earscirev.2019.01.018.
Torquato, J.R., Cordani, U.G., 1981. Brazil-Africa geological links. Earth Sci. Rev. 17, 155–176. https://doi.org/10.1016/0012-8252(81)90010-6.
Torsvik, T.H., Briden, J.C., Smethurst, M.A., 2000. Super-IAPD: InteractiveAnalysis of Palaeomagnetic Data.
Torsvik, T.H., Van der Voo, R., Preeden, U., Mac Niocaill, C., Steinberger, B., Doubrovine, P.V., van Hinsbergen, D.J.J., Domeier, M., Gaina, C., Tohver, E., Meert, J.G., McCausland, P.J.A., Cocks, L.R.M., 2012. Phanerozoic polar wander, palaeogeography and dynamics. Earth Sci. Rev. 114, 325–368. https://doi.org/10.1016/j.earscirev.2012.06.007.
Trindade, R.I.F., D'Agrella-Filho, M.S., Antonio, P.Y.J., Teixeira, W., 2021. Chapter 14 - The Precambrian drift history and paleogeography of Congo–São Francisco craton. In: Pesonen, L.J., Salminen, J., Elming, S.-Å., Evans, D.A.D., Veikkolainen, T. (Eds.), Ancient Supercontinents and the Paleogeography of Earth. Elsevier, pp.445-464. DOI: 10.1016/B978-0-12-818533-9.00016-3.
Upton, B.G.J., Rämö, O.T., Heaman, L.M., Blichert-Toft, J., Kalsbeek, F., Barry, T.L., Jepsen, H.F., 2005. The Mesoproterozoic Zig-Zag dal basalts and associated intrusions of eastern North Greenland: mantle plume–lithosphere interaction. Contrib. Miner. Petrol. 149, 40–56. https://doi.org/10.1007/s00410-004-0634-7.
Van der Voo, R., 1990. The reliability of paleomagnetic data. Tectonophysics 184, 1–9. https://doi.org/10.1016/0040-1951(90)90116-P.
Veikkolainen, T., Pesonen, L.J., 2021. Chapter 3 - Precambrian geomagnetic field—an overview. In: Pesonen, L.J., Salminen, J., Elming, S.-Å., Evans, D.A.D., Veikkolainen, T. (Eds.), Ancient Supercontinents and the Paleogeography of Earth. Elsevier, pp.81-108.DOI: 10.1016/B978-0-12-818533-9.00008-4.
Veikkolainen, T., Pesonen, L., Korhonen, K., 2014. An analysis of geomagnetic field reversals supports the validity of the Geocentric Axial Dipole (GAD) hypothesis in the Precambrian. Precambr. Res. 244, 33–41. https://doi.org/10.1016/j.precamres.2013.10.009.
Weber, F., Gauthier-Lafaye, F., Whitechurch, H., Ulrich, M., El Albani, A., 2016. The 2-ga eburnean orogeny in Gabon and the opening of the francevillian intracratonic basins: a review. C. R. Geosci. 348, 572–586. https://doi.org/10.1016/j.crte.2016.07.003.
Wingate, M.T.D., Pisarevsky, S.A., Gladkochub, D.P., Donskaya, T.V., Konstantinov, K. M., Mazukabzov, A.M., Stanevich, A.M., 2009. Geochronology and paleomagnetism of mafic igneous rocks in the Olenek Uplift, northern Siberia: Implications for Mesoproterozoic supercontinents and paleogeography. Precambrian Research 170, 256–266. https://doi.org/10.1016/j.precamres.2009.01.004.
Wu, H., Zhang, S., Li, Z.-X., Li, H., Jin, D., 2005. New paleomagnetic results from the Yangzhuang formation of the Jixian system, North China, and tectonic implications. Chin. Sci. Bull. 50, 1483–1489. https://doi.org/10.1360/982005-809.
Xu, H., Yang, Z., Peng, P., Meert, J.G., Zhu, R., 2014. Paleo-position of the North China craton within the supercontinent Columbia: Constraints from new paleomagnetic results. Precambr. Res. 255, 276–293. https://doi.org/10.1016/j.precamres.2014.10.004.
Zhang, S.-H., Ernst, R.E., Yang, Z., Zhou, Z., Pei, J., Zhao, Y., 2022. Spatial distribution of 1.4-1.3 ga LIPs and carbonatite-related REE deposits: Evidence for large-scale continental rifting in the Columbia (Nuna) supercontinent. Earth Planet. Sci. Lett. 597, 117815 https://doi.org/10.1016/j.epsl.2022.117815.
Zhao, G., Sun, M., Wilde, S.A., Li, S., 2004. A Paleo-Mesoproterozoic supercontinent: assembly, growth and breakup. Earth Sci. Rev. 67, 91–123. https://doi.org/10.1016/j.earscirev.2004.02.003.